nature chemistry

SUPPLEMENTARY INFORMATION

DOI: 10.1038/NCHEM.1707

Magnetic Relaxation Pathways in Lanthanide Single-Molecule Magnets

Robin J. Blagg,[1] Liviu Ungur,[2] Floriana Tuna,[1] James Speak,[1] Priyanka Comar,[1] David Collison,[1] Wolfgang Wernsdorfer,[3] Eric J. L. McInnes,[1] Liviu F. Chibotaru[2]* & Richard E. P. Winpenny[1]**

[1] *School of Chemistry & Photon Science Institute, The University of Manchester, Oxford Road, Manchester, M13 9PL, U.K.*

[2] *Division of Quantum and Physical Chemistry, Katholieke Universiteit Leuven, Celestijenlaan 200F, 3001 Leuven, Belgium*

[3] *Institut Néel, CNRS & UJF BP 166, 38042 Grenoble Cedex 9, France*

Table of Contents

1.0 Experimental and Synthetic Details

All reactions and manipulations were performed under an atmosphere of dry oxygen free nitrogen, using either standard Schlenk techniques or within a glove box. Toluene was dried using an Innovative Technologies solvent purification system, *n*-hexane was dried by refluxing over CaH_2 and collected *via* distillation; all solvents were stored over freshly dried 3 Å molecular sieves and degassed prior to use. Anhydrous lanthanide chlorides were purchased from Strem Chemicals Inc., KO^tBu was purchased from Sigma-Aldrich and dried *in vacuo* prior to use.

Elemental analysis were performed by the School of Chemistry MicroAnalysis laboratory at the University of Manchester; using a Flash 2000 elemental analyser (for C, H), and a Thermo iCap 6300 ICP-OES (for K, Ln).

$[Gd_4K_2O(O^tBu)_{12}]$ 1 1.32 g (5 mmol) anhydrous $GdCl_3$ and 1.68 g (15 mmol) dry KO^tBu were dissolved / suspended in *ca.* 40 cm^3 dry toluene; the mixture was heated at reflux for *ca.* 18 hours. Once cooled the toluene solution was isolated by filtration and the volatiles removed *in vacuo*, isolating the crude solid product. The product was recrystallised from a concentrated *n*-hexane solution at -30 °C, isolated as a microcrystalline solid and dried *in vacuo*, giving a yield of 0.76 g.

The compounds $[Ln_4K_2O(O^tBu)_{12}]$ (Ln = Tb **2**, Dy **3**, Ho **4**, Er **5**, Y **7**) were synthesized by analogous methods from the appropriate anhydrous metal(III) chloride. Compound **8** was prepared as described in reference N° 23 in main text, replacing anhydrous $DyCl_3$ with anhydrous YCl_3, and is indistinguishable from when originally reported by Poncelet *et al.*[(PSH+1989)]

Table S1 yield and elemental analysis (calc. for $Ln_4K_2O_{13}C_{48}H_{108}$ in parentheses) for **1 – 5** and **7**.

	yield / %	elemental analysis			
		C	H	Ln	K
$[Gd_4K_2O(O^tBu)_{12}]$ **1**	38	35.94 (36.02)	6.91 (6.80)	39.19 (39.30)	4.96 (4.89)
$[Tb_4K_2O(O^tBu)_{12}]$ **2**	25	35.64 (35.87)	6.94 (6.77)	39.42 (39.55)	4.93 (4.87)
$[Dy_4K_2O(O^tBu)_{12}]$ **3**	42	35.39 (35.55)	6.76 (6.71)	39.94 (40.08)	4.97 (4.82)
$[Ho_4K_2O(O^tBu)_{12}]$ **4**	9	35.31 (35.34)	6.74 (6.67)	40.63 (40.44)	4.62 (4.79)
$[Er_4K_2O(O^tBu)_{12}]$ **5**	28	34.97 (35.14)	6.81 (6.64)	40.46 (40.78)	4.72 (4.77)
$[Y_4K_2O(O^tBu)_{12}]$ **7**	46	43.58 (43.44)	8.17 (8.20)	26.97 (26.80)	5.73 (5.89)

1.1 ^{89}Y Nuclear magnetic resonance (NMR) spectroscopy

Solid state ^{89}Y NMR spectra of $[Y_4K_2O(O^tBu)_{12}]$ **7** and $[Y_5O(O^iPr)_{13}]$ **8** were obtained by Dr Barbara E. Gore of the School of Chemistry NMR service at the University of Manchester, using a Bruker Avance III 400 MHz spectrometer for a single-pulse/magic angle spinning experiment using a 7mm low frequency probe at *ca.* 20 °C; under the same conditions $Y(NO_3)_3{\cdot}6H_2O$ was found to give a peak at δ_Y −45 ppm.

Table S2 measured ^{89}Y chemical shifts for **7** and **8**

	δ_Y (solid state)*	δ_Y ($CDCl_3$) [PSLP1991]
$[Y_4K_2O(O^tBu)_{12}]$ **7**	+180 (2Y) +200 (2Y)	-
$[Y_5O(O^iPr)_{13}]$ **8**	+230 (4Y) +238 (1Y)	+223.0 (4Y) +219.4 (1Y)

* widths at half-height *ca.* 8 ppm (160 Hz)

1.2 Dysprosium doped Yttrium clusters

The magnetic dilution samples, $\{Dy_4K_2\}$@**7** and $\{Dy_5\}$@**8**, were obtained by combining accurately measured amounts of analytically pure dysprosium and yttrium analogues (**3** & **7** and **6** & **8** respectively) in a 1:19 molar ratio, dissolving in minimum volumes of dry *n*-hexane, and recrystallising by cooling the concentrated solutions to –30 °C, isolating the microcrystalline solid and drying to constant mass *in vacuo*.

The site substituted samples Dy@**7** and Dy@**8**, were synthesised in accordance with the synthesis of pure **7** (see above) and **8** (analogous to that reported for **6** in reference N° 23), with accurately measured 19:1 molar ratios of the yttrium(III) and dysprosium(III) chloride starting materials.

Accurate yttrium/dysprosium ratios were measured by the School of Chemistry MicroAnalysis laboratory at the University of Manchester, using a Thermo iCap 6300 ICP-OES; and resulted in dysprosium content of 5.0±0.5% for the crystalline solids obtained. Measurement of the unit cells of crystalline solids were performed on an Oxford Xcaliber-2 diffractometer using Mo Kα radiation at 100 K; with the unit cell dimensions of the doped species equivalent (within 3σ) to those observed for the pure yttrium compounds **7** (see below) and **8** (as reported by Poncelet *et al.*[PSH+1989]).

2.0 Single Crystal X-ray Crystallography

Single crystals of $[Ln_4K_2O(O^tBu)_{12}]\cdot C_6H_{14}$ were grown from *n*-hexane solutions at -30 °C, suitable crystals were selected, encapsulated in a viscous perfluoropolyether and mounted on a single crystal *X*-ray diffractometer where the crystals were cooled during data collection. **1**·C_6H_{14}, **3**·C_6H_{14}, **4**·C_6H_{14} and **7**·C_6H_{14} were collected at 100 K on an Oxford Xcaliber-2 diffractometer using Mo Kα radiation and the data reduced using Agilent Technologies CrysAlisPro; **2**·C_6H_{14} was collected at 150 K on a Bruker X8 Prospector diffractometer using Cu Kα radiation and the data reduced using Bruker APEX2 software; **5**·C_6H_{14} was collected at 100 K on beamline I19 at Diamond Light Source [(DLS-I19)] using a Rigaku Saturn Kappa diffractometer and the data reduced using Agilent Technologies CrysAlisPro. Using Olex2,[(XRAY-OLEX2)] the structures were solved with either, the ShelXS-97 [(XRAY-SHELX)] structure solution program using direct methods or the olex2.solve [(XRAY-OLEX.SOLVE)] structure solution routine using charge flipping, and then refined with the ShelXL-97 [(XRAY-SHELX)] refinement program using least squares minimisation. Data has been deposited at the Cambridge Structural Database with the following CCDC numbers:

$[Gd_4K_2O(O^tBu)_{12}].C_6H_{14}$ (**1**.C_6H_{14}), CCDC 904007;
$[Tb_4K_2O(O^tBu)_{12}].C_6H_{14}$ (**2**.C_6H_{14}), CCDC 904008;
$[Dy_4K_2O(O^tBu)_{12}].C_6H_{14}$, (**3**.$C_6H_{14}$) CCDC 904009;
$[Ho_4K_2O(O^tBu)_{12}].C_6H_{14}$ (**4**.C_6H_{14}), CCDC 904010;
$[Er_4K_2O(O^tBu)_{12}].C_6H_{14}$ (**5**.C_6H_{14}), CCDC 904011;
$[Y_4K_2O(O^tBu)_{12}].C_6H_{14}$ (**7**.C_6H_{14}), CCDC 904012.

All compounds show signs of disorder, chiefly in the methyl groups of alkoxide ligands leading to large anisotropic displacement parameters for some atoms. The C-C bond precision in these groups is therefore low in most structures, resulting in some A- and B-alerts on running the PLATON/CHEKCIF procedure.

The data for compound **4** was extremely weak due to a small crystal, and the structure is only resolved to 1.15 Å. Twinning of this crystal also led to difficulties in refinement and restraints have been added to prevent anisotropic atoms going non-positive definite; O1 in this structure was refined isotropically for this reason.

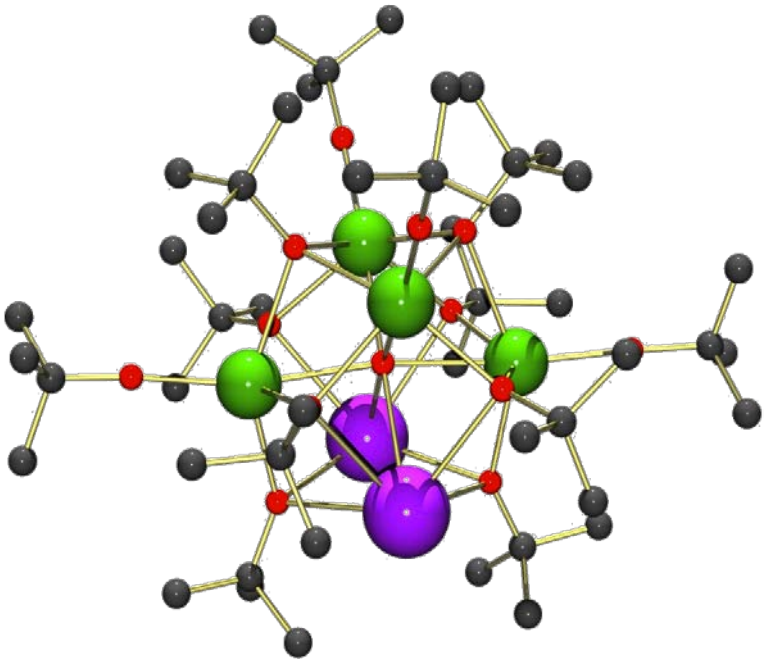

Figure S1 molecular structure of $[Dy_4K_2O(O^tBu)_{12}]$ **3**; hydrogen atoms and solvent molecule removed for clarity.

Table S3a crystallographic data for **1** - **3**

	$[Gd_4K_2O(O^tBu)_{12}]\cdot C_6H_{14}$ **1**·C_6H_{14}	$[Tb_4K_2O(O^tBu)_{12}]\cdot C_6H_{14}$ **2**·C_6H_{14}	$[Dy_4K_2O(O^tBu)_{12}]\cdot C_6H_{14}$ **3**·C_6H_{14}
empirical formula	$Gd_4K_2O_{13}C_{54}H_{122}$	$Tb_4K_2O_{13}C_{54}H_{122}$	$Dy_4K_2O_{13}C_{54}H_{122}$
formula weight	1686.72	1693.40	1707.72
temperature / K	100(2)	150(2)	100(2)
crystal system	monoclinic	monoclinic	monoclinic
space group	$P2_1/n$	$P2_1/n$	$P2_1/n$
a / Å	13.4748(5)	13.527(2)	13.4303(5)
b / Å	22.8817(7)	23.055(3)	22.9733(10)
c / Å	22.2832(7)	22.464(3)	22.2416(8)
α / °	90	90	90
β / °	92.764(3)	92.614(12)	92.340(4)
γ / °	90	90	90
volume / $Å^3$	6862.5(4)	6998.5(17)	6856.7(5)
Z	4	4	4
ρ_{calc} / $mg.mm^{-3}$	1.633	1.607	1.654
μ / mm^{-1}	3.988	20.946	4.481
F(000)	3376.0	3392.0	3408.0
crystal size / mm^3	0.3 × 0.2 × 0.1	0.1 × 0.05 × 0.05	0.3 × 0.2 × 0.1
reflections collected	23578	40980	36693
independent reflections	12562 [R(int) = 0.0701]	12772 [R(int) = 0.1599]	12519 [R(int) = 0.1051]
data / restraints / parameters	12529 / 49 / 690	12772/ 49/ 691	12519 / 39/ 688
goodness-of-fit on F^2	1.092	0.999	1.030
final R indexes [I≥2σ(I)]	R_1 = 0.0736, wR_2 = 0.1919	R_1 = 0.0852, wR_2 = 0.1973	R_1 = 0.0755, wR_2 = 0.1667
final R indexes [all data]	R_1 = 0.0930, wR_2 = 0.2037	R_1 = 0.1509, wR_2 = 0.2447	R_1 = 0.1392, wR_2 = 0.2010
largest diff. peak / hole /$e.A^{-3}$	9.33 / -7.96	2.39/ -1.57	5.84/ -3.46

Table S3b crystallographic data for **4** , **5** and **7**

	$[Ho_4K_2O(O^tBu)_{12}]\cdot C_6H_{14}$ **4**$\cdot C_6H_{14}$	$[Er_4K_2O(O^tBu)_{12}]\cdot C_6H_{14}$ **5**$\cdot C_6H_{14}$	$[Y_4K_2O(O^tBu)_{12}]\cdot C_6H_{14}$ **7**$\cdot C_6H_{14}$
empirical formula	$Ho_4K_2O_{13}C_{54}H_{122}$	$Er_4K_2O_{13}C_{54}H_{122}$	$Y_4K_2O_{13}C_{54}H_{122}$
formula weight	1717.44	1726.76	1413.36
temperature / K	100(2)	100(2)	100(2)
crystal system	monoclinic	monoclinic	monoclinic
space group	$P2_1/n$	$P2_1/n$	$P2_1/n$
a / Å	13.4449(11)	13.4621(4)	13.4872(11)
b / Å	22.959(2)	22.9237(5)	22.8936(13)
c / Å	22.217(2)	22.1745(6)	22.223(2)
α / °	90	90	90
β / °	92.434(9)	92.460(3)	92.640(7)
γ / °	90	90	90
volume / $Å^3$	6851.8(11)	6836.8(3)	6854.6(10)
Z	4	4	4
ρ_{calc} / $mg.mm^{-3}$	1.665	1.678	1.370
μ / mm^{-1}	4.742	5.033	3.526
F(000)	3424.0	3440.0	2946.0
crystal size / mm^3	0.2 × 0.1 × 0.1	0.05 × 0.05 × 0.1	0.5 × 0.3 × 0.2
reflections collected	10372	60210	26264
independent reflections	4669 [R(int) = 0.0985]	13787[R(int) = 0.1169]	12515 [R(int) = 0.2322]
data / restraints / parameters	4669/ 457 / 683	13787 / 49 / 691	12515 / 49 / 696
goodness-of-fit on F^2	1.244	1.056	1.112
final R indexes [I≥2σ(I)]	R_1 = 0.0935, wR_2 = 0.2573	R_1 = 0.0759, wR_2 = 0.1930	R_1 = 0.0935, wR_2 = 0.2160
final R indexes [all data]	R_1 = 0.1315, wR_2 = 0.2816	R_1 = 0.0868, wR_2 = 0.2044	R_1 = 0.1891, wR_2 = 0.2694
largest diff. peak / hole /$e.A^{-3}$	2.52 / -1.20	3.49 / -2.19	1.22 / -0.97

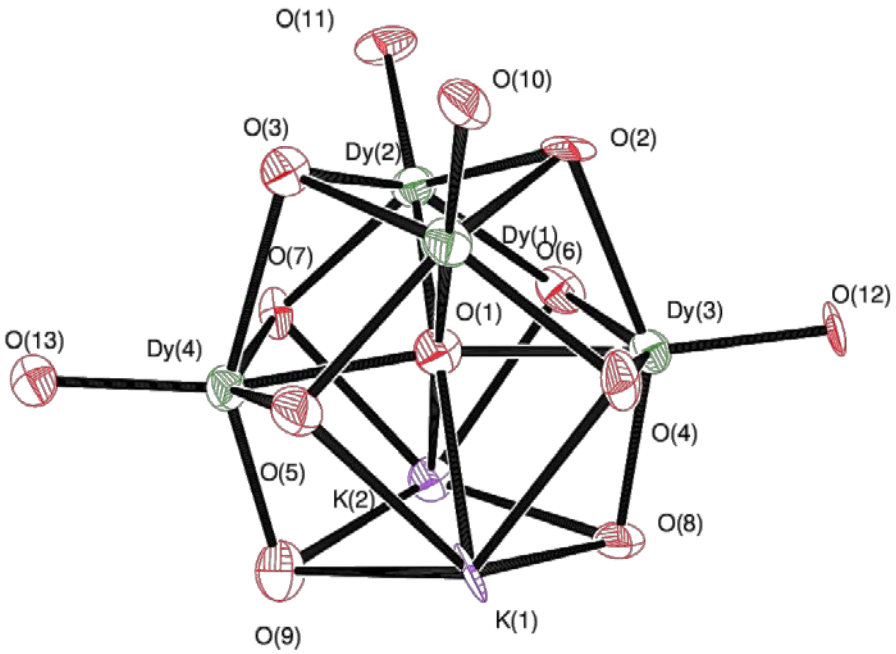

Figure S2 molecular structure of $[Dy_4K_2O(O^tBu)_{12}]$ **3** showing the numbering scheme used for all structures; thermal ellipsoids shown at 50% probability level, *tert*-butyl groups and solvent molecule removed for clarity

Table S4 metal-metal distances (Å) for **1** – **5** and **7**

	1 $\{Gd_4K_2\}$	**2** $\{Tb_4K_2\}$	**3** $\{Dy_4K_2\}$	**4** $\{Ho_4K_2\}$	**5** $\{Er_4K_2\}$	**7** $\{Y_4K_2\}$
Ln(1)···Ln(2)	3.5332(9)	3.4837(13)	3.4647(11)	3.447(3)	3.4086(7)	3.4518(15)
Ln(1)···Ln(3)	3.4930(9)	3.4577(14)	3.4208(11)	3.430(3)	3.3779(7)	3.4300(16)
Ln(1)···Ln(4)	3.5158(9)	3.4612(13)	3.4351(10)	3.419(3)	3.3797(8)	3.4378(15)
Ln(2)···Ln(3)	3.5176(9)	3.4614(13)	3.4449(11)	3.412(3)	3.3712(7)	3.4406(15)
Ln(2)···Ln(4)	3.5288(9)	3.4428(13)	3.4378(10)	3.420(2)	3.3865(7)	3.4203(15)
Ln(3)···Ln(4)	4.9049(9)	4.7948(13)	4.7528(10)	4.747(3)	4.6802(7)	4.7839(16)

Table S5 metal-oxygen bond lengths (Å) for **1** - **5** and **7**

	1 $\{Gd_4K_2\}$	**2** $\{Tb_4K_2\}$	**3** $\{Dy_4K_2\}$	**4** $\{Ho_4K_2\}$	**5** $\{Er_4K_2\}$	**7** $\{Y_4K_2\}$
K(1)–O(1)	2.726(8)	2.690(9)	2.674(9)	2.63(2)	2.683(7)	2.685(7)
K(2)–O(1)	2.631(8)	2.737(10)	2.652(9)	2.56(2)	2.623(7)	2.639(7)
Ln(1)–O(1)	2.406(8)	2.330(9)	2.324(9)	2.35(2)	2.294(6)	2.340(6)
Ln(2)–O(1)	2.387(8)	2.350(9)	2.333(8)	2.32(2)	2.305(6)	2.341(7)
Ln(3)–O(1)	2.459(8)	2.407(9)	2.378(8)	2.38(2)	2.334(7)	2.410(6)
Ln(4)–O(1)	2.458(8)	2.407(9)	2.395(8)	2.387(19)	2.363(7)	2.387(6)
Ln(1)–O(2)	2.433(9)	2.453(10)	2.415(10)	2.39(2)	2.360(8)	2.393(7)
Ln(2)–O(2)	2.405(9)	2.426(10)	2.414(10)	2.39(2)	2.379(8)	2.383(7)
Ln(3)–O(2)	2.566(9)	2.523(10)	2.515(10)	2.54(3)	2.471(8)	2.486(7)
Ln(1)–O(3)	2.418(8)	2.395(10)	2.381(10)	2.38(2)	2.363(8)	2.384(7)
Ln(2)–O(3)	2.433(9)	2.453(9)	2.421(9)	2.38(2)	2.361(8)	2.399(7)
Ln(4)–O(3)	2.504(8)	2.537(10)	2.515(9)	2.52(2)	2.480(8)	2.501(8)
K(1)–O(4)	2.790(10)	2.705(11)	2.702(10)	2.75(2)	2.786(8)	2.738(8)
Ln(1)–O(4)	2.294(9)	2.346(10)	2.305(10)	2.30(3)	2.293(8)	2.309(7)
Ln(3)–O(4)	2.398(9)	2.373(12)	2.377(10)	2.36(2)	2.341(7)	2.375(7)
K(1)–O(5)	2.836(9)	2.784(11)	2.756(11)	2.68(3)	2.721(8)	2.794(8)
Ln(1)–O(5)	2.358(8)	2.360(10)	2.333(9)	2.29(2)	2.286(8)	2.313(8)
Ln(4)–O(5)	2.375(9)	2.418(10)	2.357(10)	2.35(3)	2.334(8)	2.372(7)
K(2)–O(6)	2.757(10)	2.785(12)	2.758(11)	2.66(2)	2.666(8)	2.787(8)
Ln(2)–O(6)	2.352(9)	2.355(10)	2.343(11)	2.29(3)	2.283(8)	2.335(7)
Ln(3)–O(6)	2.416(10)	2.390(10)	2.395(10)	2.36(2)	2.329(8)	2.372(7)
K(2)–O(7)	2.734(9)	2.749(10)	2.692(11)	2.71(3)	2.720(8)	2.716(8)
Ln(2)–O(7)	2.341(8)	2.282(11)	2.321(10)	2.31(2)	2.302(8)	2.288(7)
Ln(4)–O(7)	2.391(8)	2.407(10)	2.376(10)	2.40(2)	2.353(7)	2.353(6)
K(1)–O(8)	2.730(11)	2.664(12)	2.639(11)	2.61(2)	2.657(8)	2.657(8)
K(2)–O(8)	2.633(11)	2.710(11)	2.624(11)	2.57(3)	2.639(8)	2.676(8)
Ln(3)–O(8)	2.236(9)	2.240(11)	2.233(10)	2.20(3)	2.187(8)	2.209(8)
K(1)–O(9)	2.741(10)	2.670(11)	2.678(11)	2.62(3)	2.670(10)	2.662(7)
K(2)–O(9)	2.671(11)	2.696(12)	2.611(11)	2.64(3)	2.631(9)	2.638(8)
Ln(4)–O(9)	2.230(9)	2.231(10)	2.213(11)	2.21(3)	2.183(8)	2.207(8)
Ln(1)–O(10)	2.102(9)	2.084(11)	2.091(10)	2.02(3)	2.046(8)	2.048(8)
Ln(2)–O(11)	2.100(9)	2.111(11)	2.068(10)	2.07(2)	2.080(7)	2.073(7)
Ln(3)–O(12)	2.117(10)	2.114(10)	2.089(10)	2.08(2)	2.105(8)	2.082(7)
Ln(4)–O(13)	2.113(9)	2.117(12)	2.092(9)	2.11(2)	2.089(8)	2.077(7)

Table S6 metal-oxygen bond angles (°) for **1** – **5** and **7**.

	1 $\{Gd_4K_2\}$	**2** $\{Tb_4K_2\}$	**3** $\{Dy_4K_2\}$	**4** $\{Ho_4K_2\}$	**5** $\{Er_4K_2\}$	**7** $\{Y_4K_2\}$
K(1)–O(1)–K(2)	83.0(2)	82.0(3)	81.9(3)	82.4(7)	82.46(19)	82.8(2)
K(1)–O(1)–Ln(2)	91.2(3)	90.9(3)	91.5(3)	89.9(6)	90.6(2)	90.6(2)
K(2)–O(1)–Ln(1)	174.1(4)	172.8(4)	173.3(4)	172.3(10)	173.1(3)	173.3(3)
Ln(1)–O(1)–Ln(2)	95.0(3)	96.2(3)	96.1(3)	95.2(8)	95.7(2)	95.0(2)
Ln(3)–O(1)–Ln(4)	171.8(4)	169.7(4)	169.5(4)	171.0(11)	170.3(3)	171.7(3)
O(1)–Ln(1)–O(10)	170.8(3)	174.7(4)	171.2(4)	174.5(11)	174.9(3)	175.4(3)
O(1)–Ln(2)–O(11)	175.1(3)	170.6(4)	175.3(4)	172.1(10)	171.4(3)	171.8(3)
O(1)–Ln(3)–O(12)	169.9(3)	167.2(4)	169.0(4)	170.3(9)	169.0(3)	168.6(3)
O(1)–Ln(4)–O(13)	168.4(3)	168.4(4)	167.8(3)	168.4(9)	167.8(3)	169.8(3)
O(2)–Ln(1)–O(5)	141.2(3)	143.6(3)	142.7(3)	142.9(9)	143.6(3)	142.7(2)
O(3)–Ln(1)–O(4)	141.5(3)	143.3(3)	143.4(3)	143.1(9)	143.6(3)	143.6(2)
O(2)–Ln(2)–O(7)	141.5(3)	144.1(3)	143.0(3)	143.9(9)	143.1(3)	142.5(2)
O(3)–Ln(2)–O(6)	140.9(3)	142.4(3)	142.7(3)	142.7(9)	142.6(3)	142.8(2)
O(2)–Ln(3)–O(8)	147.5(3)	150.3(3)	149.8(3)	148.4(8)	150.9(3)	148.9(3)
O(4)–Ln(3)–O(6)	141.6(3)	144.0(4)	144.2(4)	143.2(9)	144.7(3)	143.8(2)
O(3)–Ln(4)–O(9)	147.0(3)	150.1(4)	149.6(4)	149.4(9)	150.5(3)	148.8(2)
O(5)–Ln(4)–O(7)	141.6(3)	143.6(3)	144.0(3)	143.2(8)	144.5(3)	143.1(3)
O(2)–Ln(1)–O(3)	79.6(3)	81.4(3)	81.1(3)	79.6(8)	80.7(3)	80.6(2)
O(3)–Ln(1)–O(5)	79.5(3)	81.2(3)	81.1(3)	81.8(9)	81.2(3)	80.5(2)
O(5)–Ln(1)–O(4)	94.7(3)	94.3(4)	93.1(4)	95.4(9)	96.4(3)	95.8(3)
O(4)–Ln(1)–O(2)	82.0(3)	81.1(4)	82.2(3)	81.1(9)	80.4(3)	81.1(2)
O(2)–Ln(2)–O(3)	79.9(3)	80.8(3)	80.3(3)	79.7(8)	80.3(3)	80.5(2)
O(3)–Ln(2)–O(7)	79.5(3)	82.8(3)	81.8(3)	83.0(8)	81.7(3)	81.5(3)
O(7)–Ln(2)–O(6)	95.1(3)	93.2(4)	94.5(4)	92.3(9)	93.5(3)	94.7(3)
O(6)–Ln(2)–O(2)	81.1(3)	81.0(3)	81.0(4)	83.0(9)	81.9(3)	80.6(2)
O(2)–Ln(3)–O(4)	77.3(3)	79.2(3)	78.7(3)	77.1(9)	77.2(3)	77.9(2)
O(4)–Ln(3)–O(8)	96.9(3)	92.7(4)	94.8(4)	92.9(9)	93.7(3)	93.8(3)
O(8)–Ln(3)–O(6)	90.2(3)	93.0(4)	91.9(4)	93.6(10)	94.5(3)	93.3(3)
O(6)–Ln(3)–O(2)	76.7(3)	78.4(3)	77.9(3)	78.6(9)	79.1(3)	77.8(2)
O(3)–Ln(4)–O(5)	77.5(3)	77.3(3)	77.9(3)	77.7(9)	77.8(3)	77.0(2)
O(5)–Ln(4)–O(9)	93.8(3)	91.6(4)	93.8(4)	92.8(10)	94.9(3)	92.2(3)
O(9)–Ln(4)–O(7)	92.1(3)	95.9(4)	92.7(4)	93.7(10)	93.2(3)	95.1(3)
O(7)–Ln(4)–O(3)	77.1(3)	78.6(3)	78.7(3)	78.4(9)	78.2(3)	78.2(2)

3.0 SQUID Magnetometry

The magnetic properties of polycrystalline samples were investigated in the temperature range 1.8-300 K, by using a Quantum Design MPMS XL SQUID magnetometer equipped with a 7 T magnet. Data were corrected for the diamagnetism of the compounds by using Pascal's constants and for the diamagnetic contribution of the sample holder by measurement. Alternating current (ac) susceptibility measurements were performed with an ac field of 1.55 G oscillating at frequencies between 1 and 1400 Hz.

Table S7 summary of direct current (dc) magnetic data for **1**-**5**.

	1 (Gd)	**2** (Tb)	**3** (Dy)	**4** (Ho)	**5** (Er)
ground state term of Ln^{III} ion	$^8S_{7/2}$	$^7F_6$	$^6H_{15/2}$	$^5I_8$	$^4I_{15/2}$
C ($cm^3.K.mol^{-1}$) for each Ln^{III} ion	7.88	11.82	14.17	14.07	11.48
$\chi_M T$ ($cm^3.K.mol^{-1}$) expected value for four non-interacting Ln^{III} at room temperature	31.52	47.28	56.68	56.28	45.92
$\chi_M T$ ($cm^3.K.mol^{-1}$) experimental value for $\{Ln_4\}$ at 300 K	31.68	48.60	56.34	56.35	48.32
$\chi_M T$ ($cm^3.K.mol^{-1}$) experimental value for $\{Ln_4\}$ at 2 K	9.82	14.30	30.03	34.37	23.26
magnetization (μ_B) observed at 7 T and 2 K	27.90	19.73	21.43	21.87	21.00

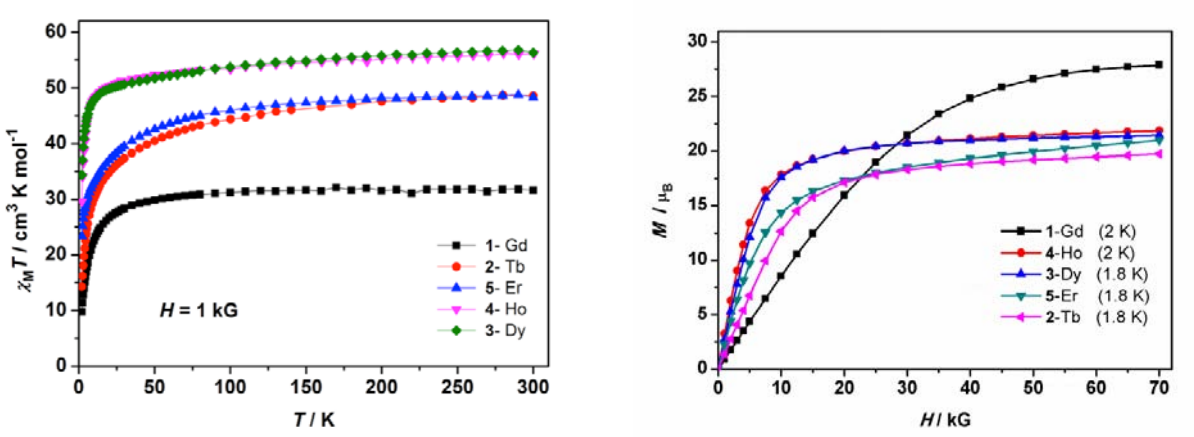

Figure S3 Plots of (left) $\chi_m T$ *vs*. T and (right) M vs. H for compounds **1** - **5**.

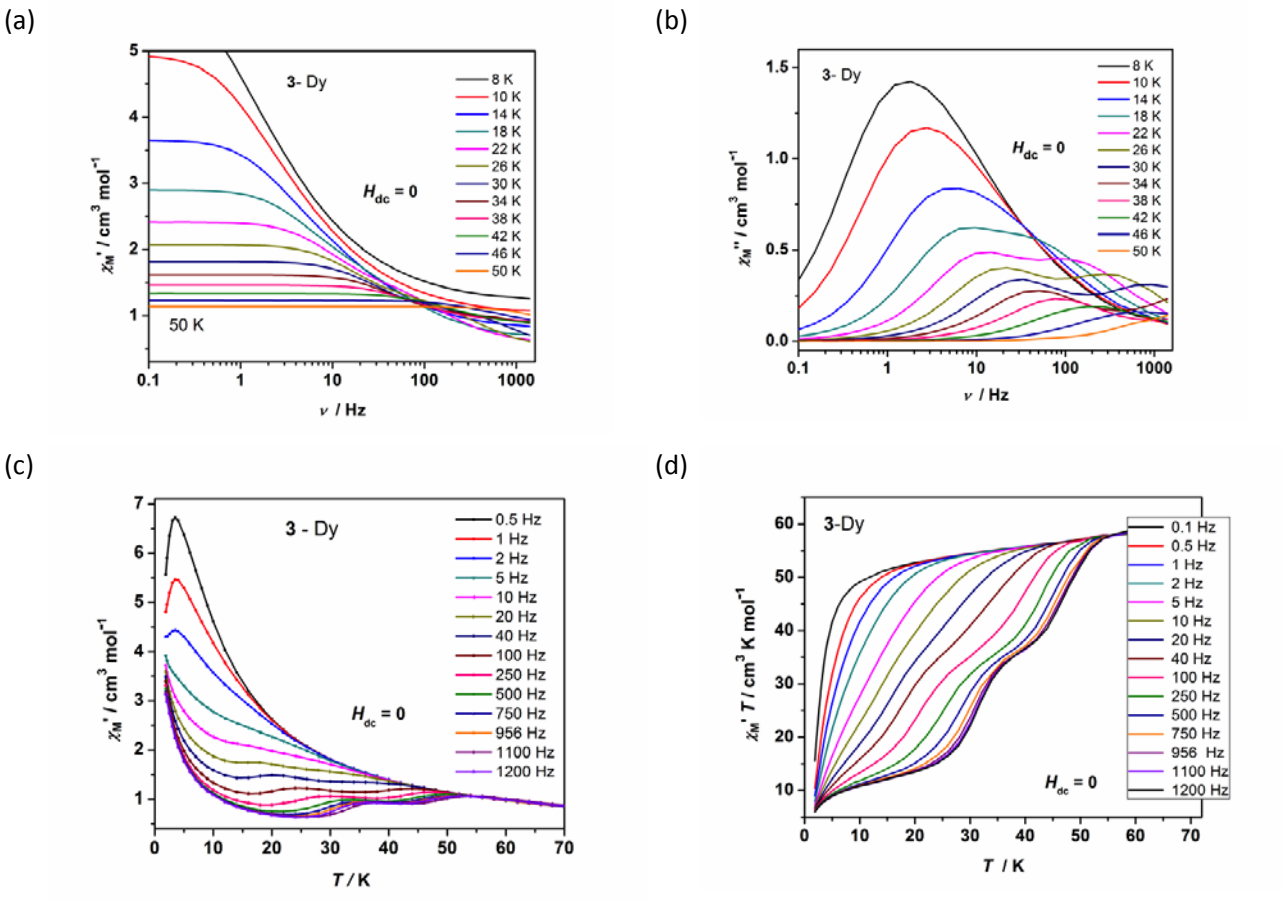

Figure S4 Frequency- dependence at zero dc-field of the (a) in-phase (χ_M') and (b) out-of phase (χ_M'') ac susceptibilities of **3** at temperatures between 8 and 50 K. Temperature dependence at zero dc field of (c) χ_M' and (d) $\chi_M'T$ for **3** at frequencies between 0.5 and 1200 Hz.

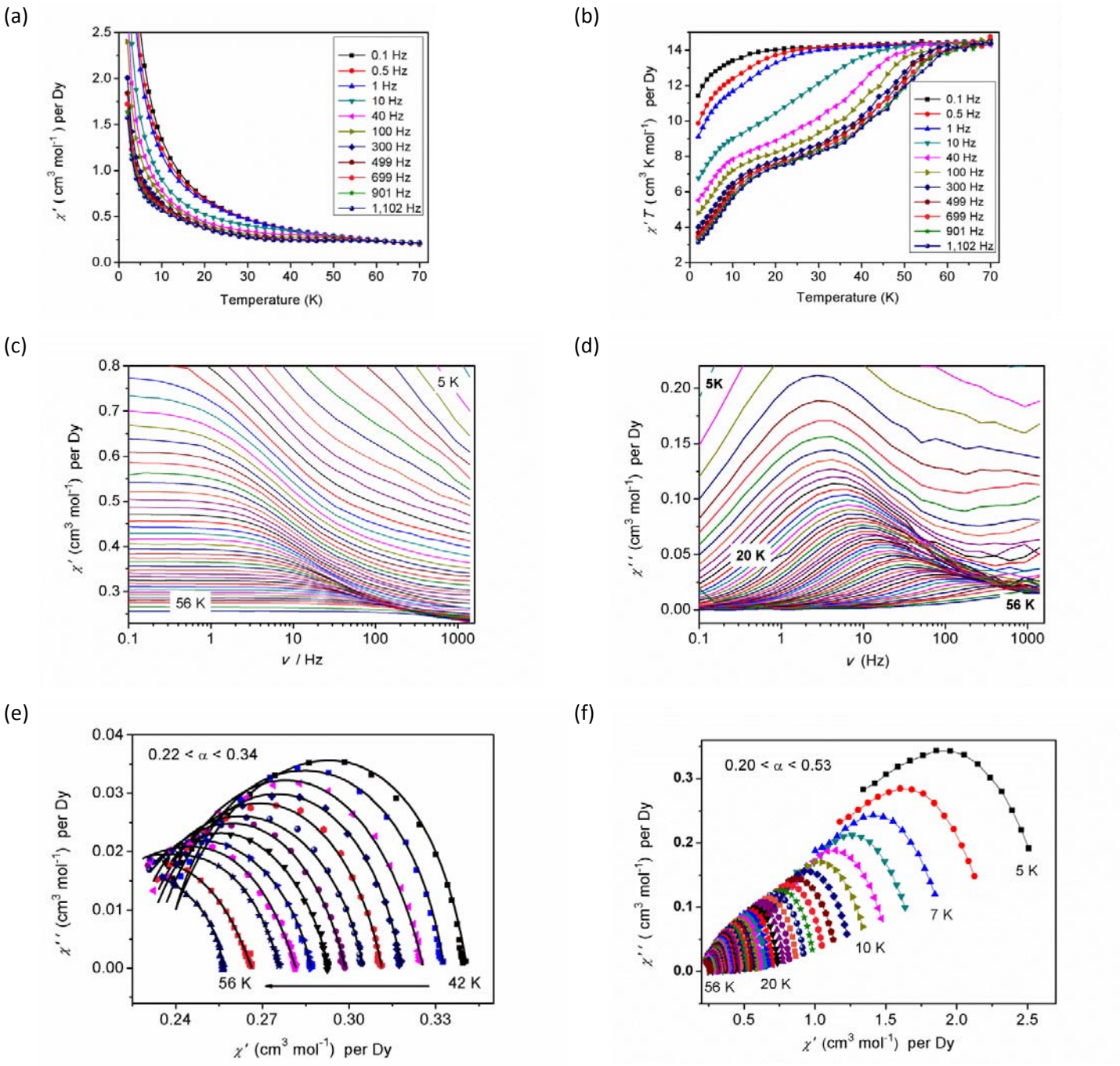

Figure S5 (a) χ' (T) and (b) $\chi'T\,(T)$ of Dy@ **7** at H_{dc} = 0, H_{ac} = 1.55 Oe and frequencies in the range 0.1 -1,202 Hz. (c) $\chi'(\nu)$, (d) $\chi''\,(\nu)$ and (e) and (f) $\chi''\,(\chi')$ of Dy@**7** at H_{dc} = 0, H_{ac} = 1.55 Oe and frequencies in the range 0.1 -1,400 Hz.

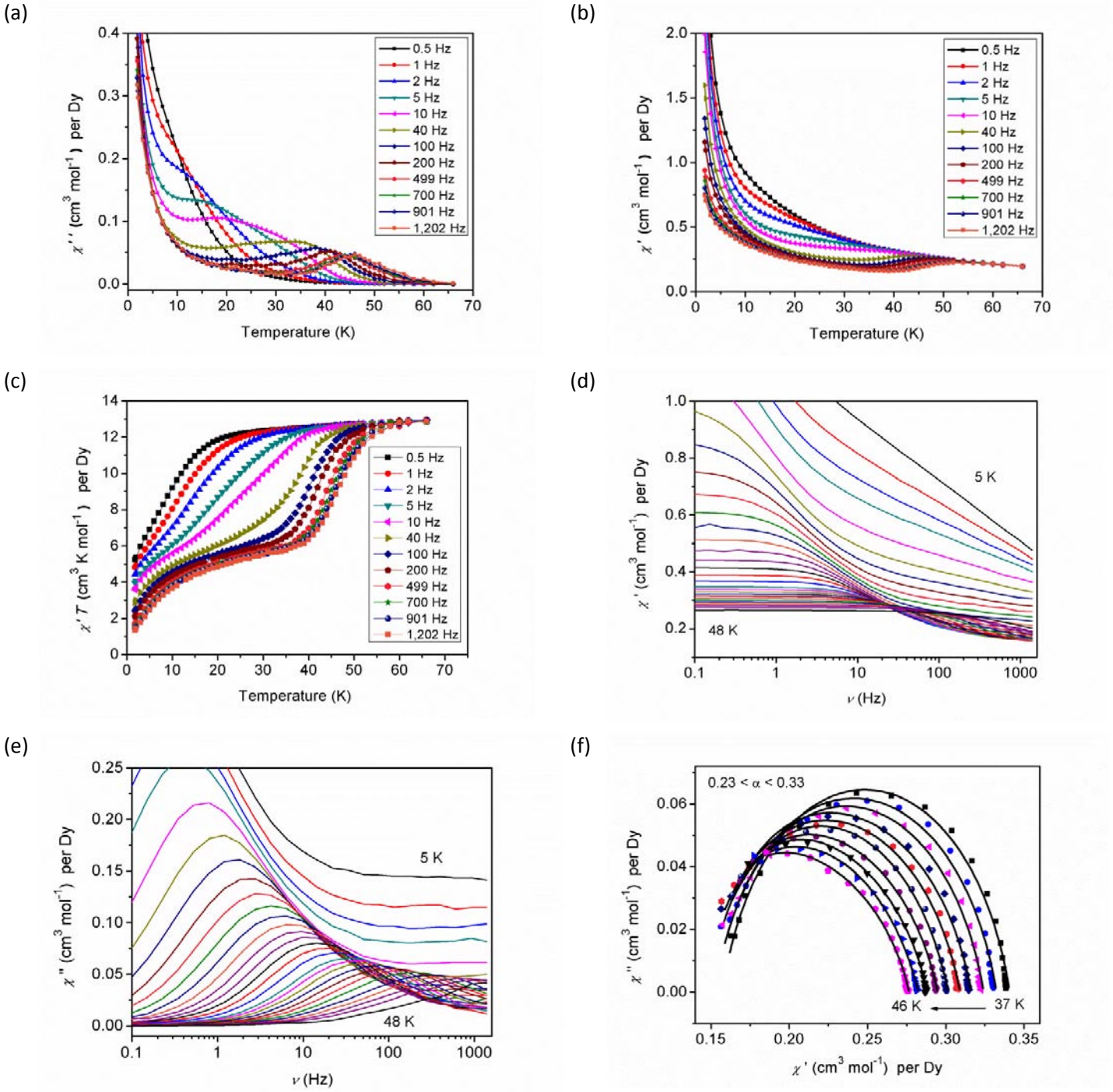

Figure S6 (a) $\chi''(T)$, (b) χ' (T) and (c) $\chi'T(T)$ and of Dy@ **8** at H_{dc} = 0, H_{ac} = 1.55 Oe and frequencies in the range 0.5 - 1,202 Hz. (d) $\chi'(\nu)$, (e) $\chi''(\nu)$ and (f) $\chi''(\chi')$ of Dy@**8** at H_{dc} = 0, H_{ac} = 1.55 Oe and frequencies in the range 0.1 -1,400 Hz

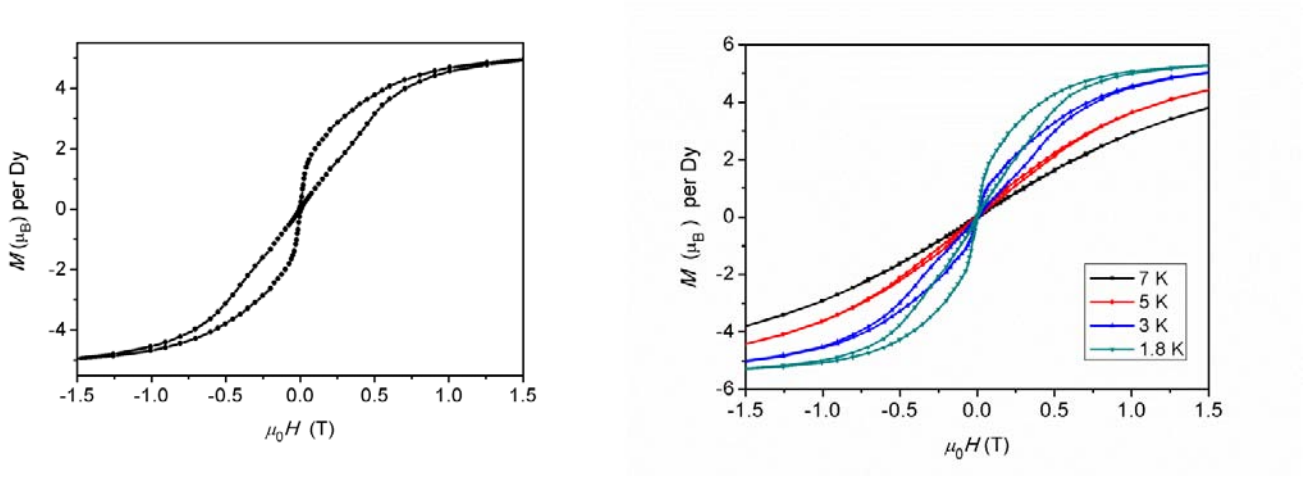

Figure S7 *M*(*H*) of Dy@**7** at temperatures from 1.8 to 7 K.

(a)

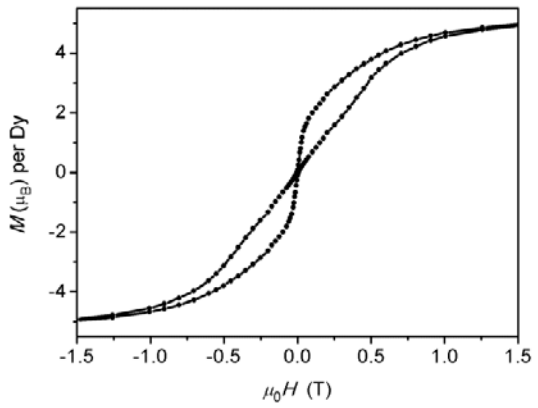

(b)

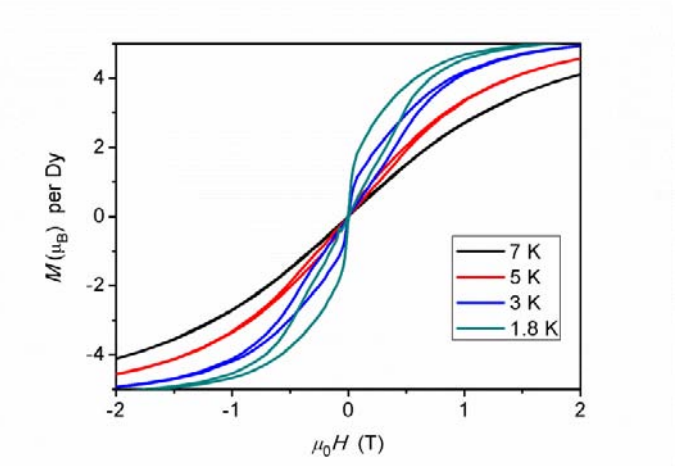

(c)

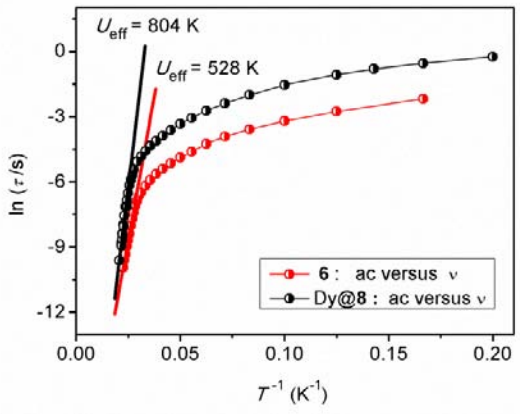

Figure S8 (a) and (b) *M*(*H*) of Dy@**8** at temperatures from 1.8 to 7 K. (c) ln τ *vs.* T^{-1} of **6** and Dy@**8**

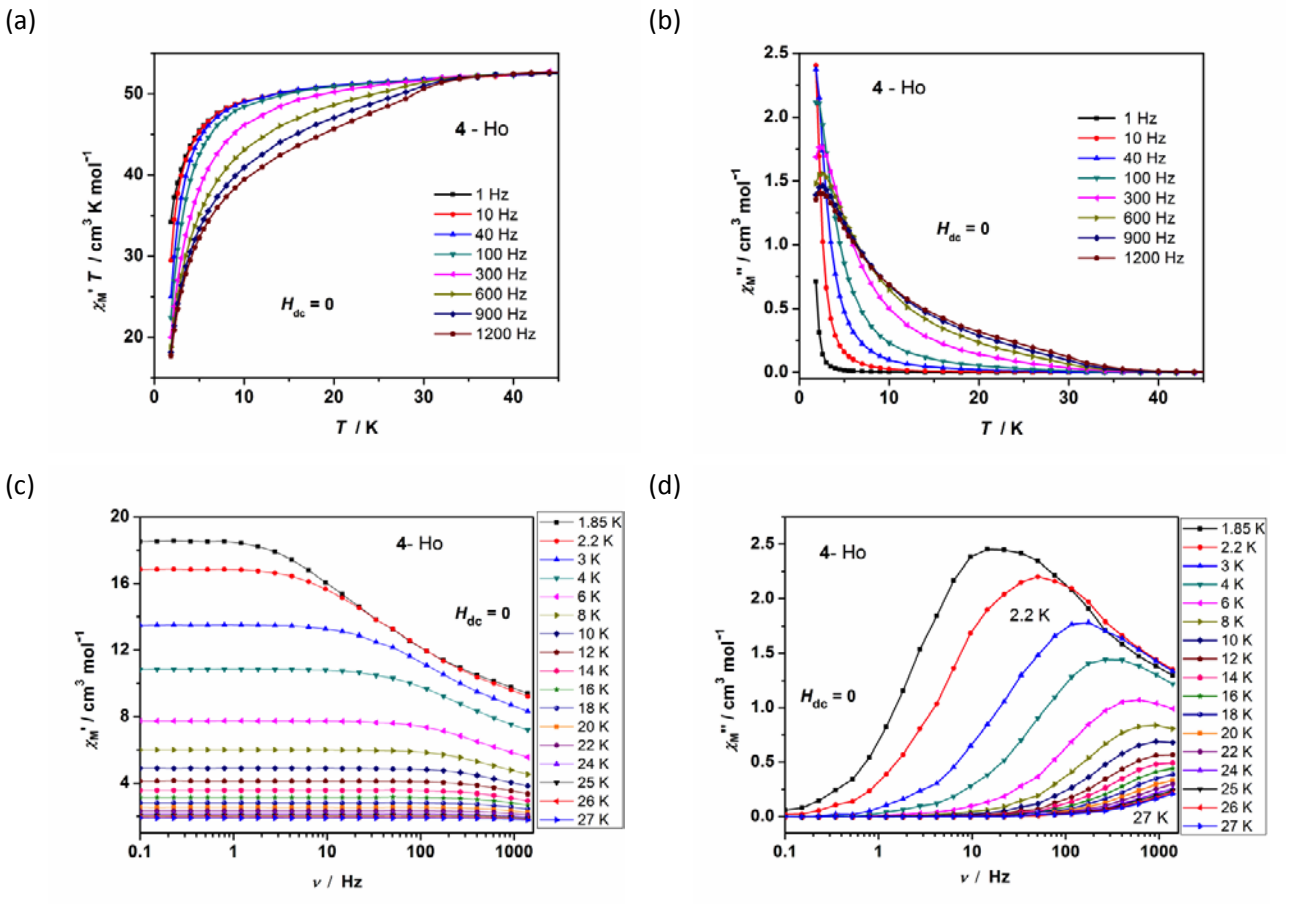

Figure S9 Temperature dependence at zero dc field of (a) χ_M' and (b) χ_M'' for **4** at frequencies between 1 and 1200 Hz. Frequency- dependence at zero dc-field of (c) χ_M' and (d) χ_M'' for **4** at temperatures between 1.8 and 27 K.

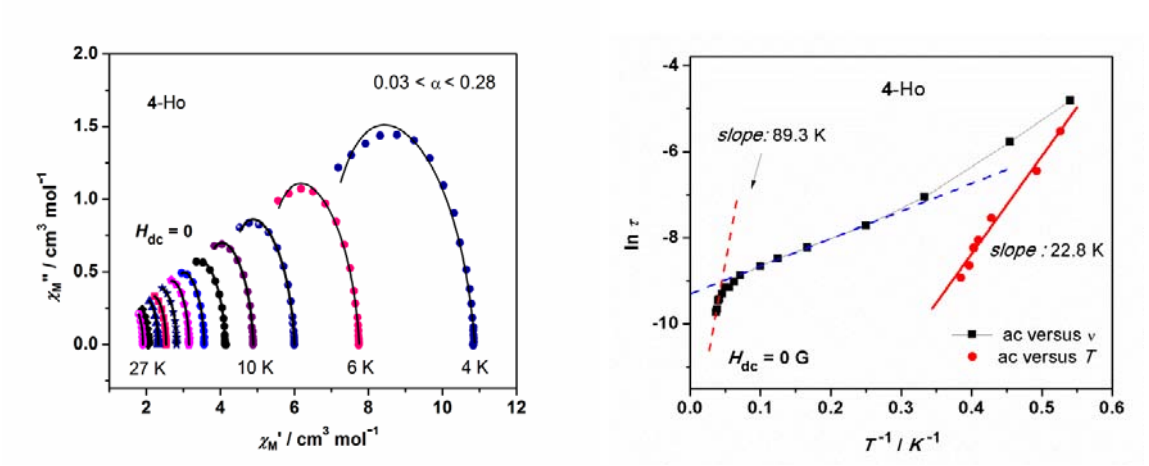

Figure S10 *Left:* Cole-Cole plots for **4** at temperatures between 4 and 27 K, zero-dc field and frequencies between 1 and 1400 Hz. *Right:* Plot of ln τ *vs.* T^{-1} for 4 at zero- dc field.

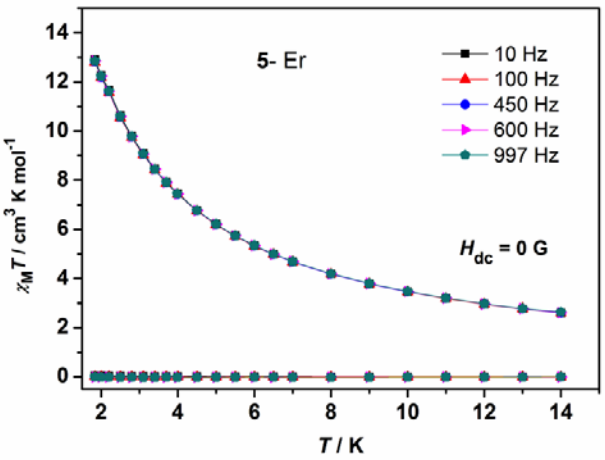

***Figure S*11** Temperature dependence of the out-of-phase ac susceptibility of **5** at zero- dc field and frequencies from 10 to 997 Hz.

4.0 Quantum Chemical Calculations

4.1 Computational Details

All calculations were done with MOLCAS 7.6 and are of CASSCF/RASSI/SINGLE_ANISO type. For Er and Ho fragments we mixed all spin states by the spin coupling, while for Dy only a limited number of roots could possibly be mixed, namely 21 sextet, 128 quartet and 130 doublet states. From the resulting spin-orbital multiplets, the SINGLE_ANISO program computes single ion magnetic properties (*g*-tensors, main magnetic axes, local magnetic susceptibility, etc.). Further, the exchange interaction between magnetic centres was computed by the POLY_ANISO program (reference 18 main text).

Three structural approximations of the initial Ln_4K_2 molecules were employed **A**, **B** and **C**.
In the structural model **A**, all *tert*-butyl fragments were replaced by H;
In the structural model **B**, all *tert*-butyl fragments were replaced by CH_3;
In the structural model **C**, the entire molecule was computed *ab initio*;
The structures of the models **A** and **B** are shown in Figures S12 and S13.

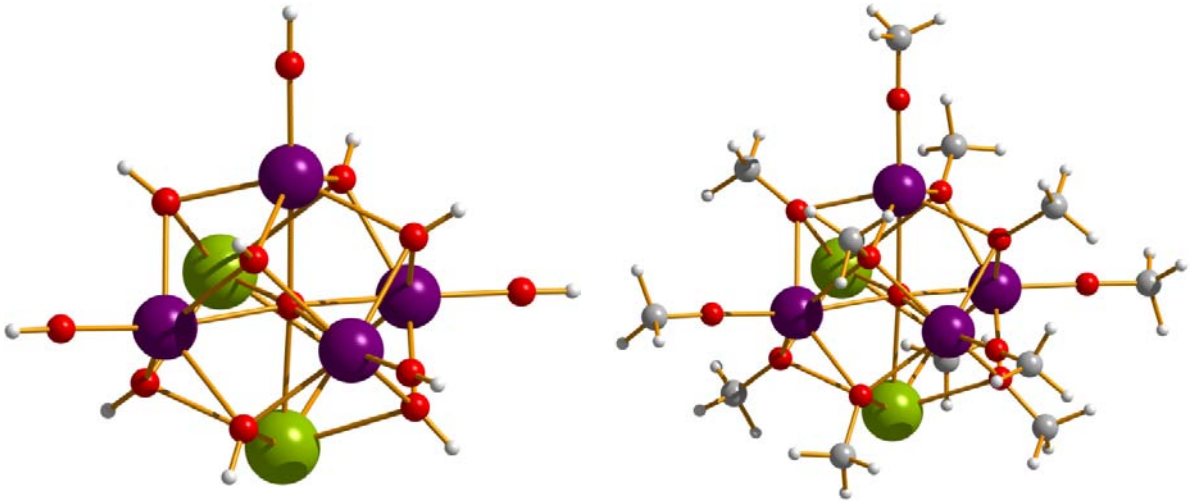

Figure S12 Structure of the model A (right) and B (left) of the $\{Dy_4K_2\}$ molecule.

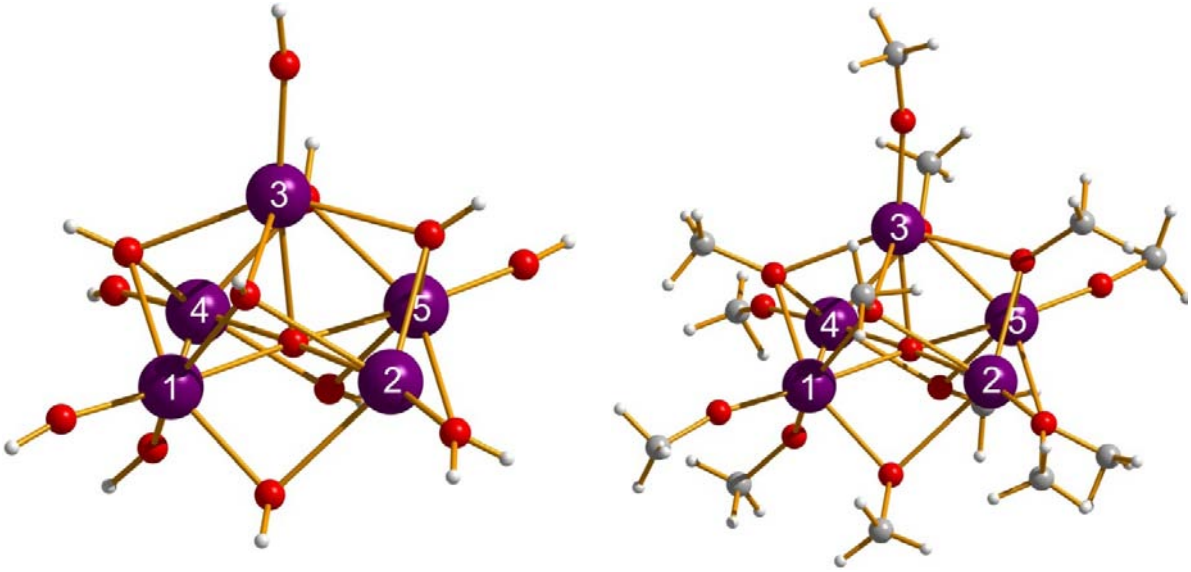

Figure S13 Structure of the model A (right) and B (left) of the $\{Dy_5\}$ molecule.

The mononuclear Ln fragments have the same structure as the initial structural model of the $\{Ln_4K_2\}$ (**A**, **B** or **C**), in which all other three Ln ions were computationally substituted by diamagnetic Lu.

Three basis set approximations have been employed: **1** – small, **2** – medium and **3**- large; Table S8 shows the contractions of the employed basis sets for all elements.

All in all there are 9 computational models for each magnetic centre in a molecule:
A1, **A2**, **A3**, **B1**, **B2**, **B3**, **C1**, **C2**, and **C3**.
The results do not differ much, and the obtained solution for each centre is stable for all computational approximations.

Table S8 Contractions of the employed basis sets in computational approximations 1 - 3.

a employed for models A and B:

Basis 1	Basis 2	Basis 3
Ln.ANO-RCC...7s6p4d3f1g.	Ln.ANO-RCC...7s6p4d3f1g.	Ln.ANO-RCC...8s7p5d4f2g1h.
Lu.ANO-DK3.Tsuchiya.27s23p15d10f.6s4p3d1f.	Lu.ANO-RCC...7s6p4d3f1g.	Lu.ANO-RCC...7s6p4d3f1g.
K.ANO-DK3.Tsuchiya.20s15p.4s2p.	K.ANO-RCC...5s4p1d.	K.ANO-RCC...5s4p1d.
O.ANO-RCC...3s2p1d. (close)	O.ANO-RCC...3s2p1d. (close)	O.ANO-RCC...4s3p2d. (close)
O.ANO-DK3.Tsuchiya.12s8p.2s1p. (distant)	O.ANO-RCC...3s2p. (distant)	O.ANO-RCC...3s2p. (distant)
C.ANO-RCC...3s2p. (close)	C.ANO-RCC...3s2p1d. (close)	C.ANO-RCC...4s3p2d. (close)
C.ANO-DK3.Tsuchiya.12s8p.2s1p. (distant)	C.ANO-DK3.Tsuchiya.12s8p.2s1p. (distant)	C.ANO-RCC...3s2p. (distant)
H.ANO-RCC...2s. (close)	H.ANO-RCC...2s. (close)	H.ANO-RCC...2s1p. (close)
H.ANO-DK3.Tsuchiya.6s.1s. (distant)	H.ANO-DK3.Tsuchiya.6s.1s. (distant)	H.ANO-RCC...2s. (distant)

b employed for model C:

Basis 1	Basis 2	Basis 3
Ln.ANO-RCC...7s6p4d3f1g.	Ln.ANO-RCC...7s6p4d3f1g.	Ln.ANO-RCC...8s7p5d4f2g1h.
Lu.ANO-DK3.Tsuchiya.27s23p15d10f.6s4p3d1f.	Lu.ANO-RCC...7s6p4d3f1g.	Lu.ANO-RCC...7s6p4d3f1g.
K.ANO-DK3.Tsuchiya.20s15p.4s2p.	K.ANO-RCC...5s4p1d.	K.ANO-RCC...5s4p1d.
O.ANO-RCC...3s2p1d. (close)	O.ANO-RCC...3s2p1d. (close)	O.ANO-RCC...4s3p2d. (close)
O.ANO-DK3.Tsuchiya.12s8p.2s1p. (distant)	O.ANO-RCC...3s2p. (distant)	O.ANO-DK3.Tsuchiya.12s8p.2s1p. (distant)
C.ANO-RCC...3s2p. (close)	C.ANO-RCC...3s2p1d. (close)	C.ANO-RCC...3s2p1d. (close)
C.ANO-DK3.Tsuchiya.12s8p.2s1p. (distant)	C.ANO-DK3.Tsuchiya.12s8p.2s1p. (distant)	C.ANO-DK3.Tsuchiya.12s8p.2s1p. (distant)
H.ANO-RCC...2s. (close)	H.ANO-RCC...2s. (close)	H.ANO-DK3.Tsuchiya.6s.1s.
H.ANO-DK3.Tsuchiya.6s.1s. (distant)	H.ANO-DK3.Tsuchiya.6s.1s. (distant)	

Active space of the CASSCF method includes the electrons from the last shell spanning the 7 orbitals (4*f* orbitals of the Ln^{3+} ion).

For Dy only a limited number of roots was possible to mix, namely 21 sextets, 128 quartet and 130 doublet states. On the basis of the resulting spin-orbital multiplets the SINGLE_ANISO program computed local magnetic properties (*g*-tensors, main magnetic axes, local magnetic susceptibility, etc.)

Further, the exchange interaction between magnetic centers was computed by the POLY_ANISO program.

All calculations presented below correspond to the highest computational approximation C3.

Calculations with approximations (**A1**-**C2**), not shown in this ESI, have been done for the sake of checking the stability of the obtained CASSCF self-consistent solutions for Ln fragments of investigated complexes. These results are available on request from the authors (L.U. and L.F.C.)

4.2 Ab initio studies of the {Dy_4K_2} and {Dy_5} complexes

Table S9. Calculated energies of states 2± and 3± for individual Dy sites in compounds **3** and **6** and the angle (ϕ_{12}) between the main anisotropy axis of state 1± and state 2±.

Compound	Ln site	Energy of state 2± / K	Energy of state 3± / K	ϕ_{12} /°
3	Dy1	552	956	0.71
3	Dy2	582	1041	0.73
3	Dy3	515	799	2.73
3	Dy4	496	754	0.92
6	Dy1	622	1033	2.91
6	Dy2	595	1127	1.07
6	Dy3	580	1064	1.33
6	Dy4	491	877	3.37
6	Dy5	591	830	1.88

Table S10 Energies (cm^{-1}) of the low lying Kramers doublets in compounds {Dy_4K_2} **3** and {Dy_5} **6**.

{Dy_4K_2}				{Dy_5}				
Dy1	**Dy2**	**Dy3**	**Dy4**	**Dy1**	**Dy2**	**Dy3**	**Dy4**	**Dy5**
0.000	0.000	0.000	0.000	0.000	0.000	0.000	0.000	0.000
383.862	404.677	358.088	344.426	431.980	413.366	402.818	341.379	410.855
664.336	723.499	555.587	523.975	718.265	783.468	739.458	609.595	576.874
737.773	830.621	623.294	590.065	807.173	1033.826	933.988	683.999	679.287
811.875	901.010	721.078	665.074	874.603	1114.652	1000.974	741.879	732.782
880.518	960.915	766.449	729.271	987.160	1149.299	1032.412	824.212	853.562
941.588	1017.703	843.349	791.049	1044.886	1215.082	1096.035	859.716	940.731
1042.734	1113.027	919.844	828.532	1175.703	1268.355	1199.808	925.682	1031.652
3751.639	3765.712	3736.202	3728.713	3787.972	3771.721	3765.660	3722.425	3776.210
4020.621	4065.557	3964.184	3939.820	4056.598	4126.630	4081.101	3990.516	3999.720
4179.305	4239.801	4101.572	4071.840	4234.890	4333.353	4274.136	4131.358	4144.731
4276.876	4342.590	4167.522	4140.776	4358.043	4483.382	4408.611	4216.979	4222.619
4345.259	4421.545	4232.591	4185.403	4436.181	4609.884	4511.498	4274.962	4290.609
4397.044	4470.713	4297.701	4248.525	4498.354	4696.585	4578.173	4331.925	4364.317
4463.991	4558.005	4353.982	4264.314	4553.621	4749.436	4653.763	4367.176	4414.473
6449.606	6484.687	6407.168	6392.573	6488.950	6511.879	6487.906	6409.443	6451.378
6548.114	6598.212	6487.635	6460.906	6595.564	6682.602	6630.529	6515.853	6521.196
6660.245	6710.877	6589.725	6557.115	6728.022	6832.891	6769.694	6610.228	6638.234
6780.893	6841.485	6689.985	6649.708	6866.716	6995.259	6920.169	6713.728	6746.250
6895.366	6972.679	6777.410	6730.420	6986.480	7162.681	7064.879	6825.326	6832.556
6984.796	7080.090	6875.441	6802.592	7067.074	7278.469	7170.365	6908.229	6930.342
8475.863	8525.151	8416.505	8395.972	8505.006	8586.117	8547.369	8434.576	8436.904
8518.975	8568.151	8457.044	8429.862	8585.504	8670.905	8612.846	8481.533	8505.061
8633.227	8682.618	8562.251	8524.148	8705.753	8823.181	8756.462	8577.730	8609.508
8782.413	8851.911	8681.169	8637.013	8868.541	9019.878	8937.480	8712.105	8729.568
8914.068	9005.906	8802.770	8738.036	8992.466	9198.281	9092.683	8845.730	8855.624
10020.286	10076.721	9956.200	9935.514	10047.722	10160.170	10114.139	9980.495	9973.484
10058.624	10099.512	10000.436	9969.992	10128.666	10207.480	10149.138	10018.788	10041.628
10250.429	10310.855	10164.570	10122.618	10337.424	10473.769	10399.198	10179.030	10211.194
10418.750	10474.839	10315.858	10253.608	10477.103	10607.518	10536.557	10362.030	10355.249

Table S11 Main values of the *g* tensors of the low-lying Kramers doublets on Dy sites in compounds $\{Dy_4K_2\}$ **3** and $\{Dy_5\}$ **6**.

	KD	$\{Dy_4K_2\}$				$\{Dy_5\}$				
		Dy1	**Dy2**	**Dy3**	**Dy4**	**Dy1**	**Dy2**	**Dy3**	**Dy4**	**Dy5**
1	g_X	0.00029	0.00019	0.00016	0.00027	0.00039	0.00001	0.00003	0.00047	0.00117
	g_Y	0.00055	0.00032	0.00039	0.00054	0.00073	0.00001	0.00007	0.00063	0.00231
	g_Z	19.87283	19.88353	19.89131	19.89089	19.85970	19.89187	19.88316	19.87541	19.84431
2	g_X	0.06125	0.03339	0.13875	0.18193	0.07287	0.00139	0.01103	0.03805	0.28138
	g_Y	0.06414	0.03447	0.19039	0.23157	0.08001	0.00146	0.01145	0.04324	0.45540
	g_Z	16.95769	16.99443	16.87407	16.79062	16.85384	17.05065	17.03399	17.02125	16.47147
3	g_X	0.86911	0.39147	2.54973	1.65078	0.47007	0.06138	0.06770	0.20569	1.50454
	g_Y	2.20150	0.87617	4.26076	2.30727	0.93826	0.06460	0.13018	0.54465	2.24824
	g_Z	12.40966	13.38587	14.63234	15.06339	13.03512	14.25206	14.09812	12.89568	16.36609
4	g_X	11.87931	2.10804	7.77596	9.44584	10.64238	0.66815	8.62956	11.86627	1.84133
	g_Y	6.69792	6.28844	6.29499	6.37625	7.42970	1.27554	7.00193	7.30124	4.58436
	g_Z	1.40724	13.10685	0.30667	2.98280	2.26800	11.21259	4.18289	2.17679	12.10859
5	g_X	0.61102	0.56645	1.19462	1.47992	1.51793	1.87768	0.13063	11.86627	1.85636
	g_Y	5.67895	3.62450	3.53331	3.77550	3.28873	6.66484	5.95426	7.30124	2.70834
	g_Z	12.56535	14.58101	15.54775	13.72901	12.00042	12.38914	12.66704	2.17679	14.00756
6	g_X	8.88869	6.84395	1.24377	10.55602	8.13877	0.55337	2.15405	8.54961	0.47380
	g_Y	7.93553	5.45939	3.61558	6.82221	6.53281	3.40915	2.70550	6.86960	3.95425
	g_Z	2.62617	1.81249	13.41230	1.78994	1.26212	13.17622	9.29175	4.05588	12.88248
7	g_X	1.10835	10.91836	0.40335	0.32912	2.47435	2.19619	2.63717	1.92315	1.35246
	g_Y	1.93124	6.97970	1.02801	3.14887	5.04977	4.80325	5.45002	2.83084	2.93339
	g_Z	15.29008	2.18518	15.02482	13.68359	13.55637	10.91149	13.80887	15.78871	12.85980
8	g_X	0.14615	0.49384	0.25061	0.50389	0.02712	0.88546	0.06340	0.38726	0.30631
	g_Y	0.59534	0.94484	0.78986	3.56082	0.31499	2.50987	0.12740	1.05531	1.05404
	g_Z	18.55878	18.66529	18.00745	15.84469	18.57565	16.57501	19.18962	17.78468	17.36739

Table S12 Angle between the main magnetic axis of the ground Kramers doublets (KD 1) and the shortest chemical bond (Dy-O) of the corresponding Dy site in compounds $\{Dy_4K_2\}$ **3** and $\{Dy_5\}$ **6**.

$\{Dy_4K_2\}$				$\{Dy_5\}$				
Dy1	**Dy2**	**Dy3**	**Dy4**	**Dy1**	**Dy2**	**Dy3**	**Dy4**	**Dy5**
0.5486	0.6960	2.7273	2.3071	5.7899	4.1109	2.6623	4.6910	5.2371

4.3 Ab initio calculations for Dy_4K_2 (3) in the presence of electrostatic intermolecular interaction

The results in the Tables S13-S15 are obtained for the same molecular structures and approximation (C3) as in Tables S9-S12 but with additional account of the electrostatic field of Mulliken charges of all atoms of surrounding molecules. Given the electric neutrality of each molecule, the electrostatic electric field generated by them is of dipolar (and higher polarity) type, i.e., decreases quickly with the intermolecular separation, which justifies the use of only four layers of unit cells for simulation of Madelung potential.

Table S13. Energies (cm^{-1}) of the low-lying Kramers doublets in Dy_4K_2 (3)

Dy_4K_2			
Dy1	**Dy2**	**Dy3**	**Dy4**
0.000	0.000	0.000	0.000
384.382	405.722	357.842	349.782
660.416	722.622	549.959	537.959
731.334	828.341	617.589	596.625
800.153	897.079	713.342	671.886
872.638	957.614	758.219	738.354
932.362	1014.049	834.913	798.459
1028.567	1111.982	912.203	833.397
3755.031	3769.155	3738.835	3734.771
4019.211	4065.965	3963.155	3946.714
4177.315	4240.414	4099.271	4082.128
4273.998	4343.390	4163.525	4152.401
4339.343	4421.599	4228.081	4194.872
4388.482	4468.811	4291.694	4258.078
4452.709	4559.116	4347.085	4273.434
6452.676	6488.596	6409.225	6402.193
6547.998	6600.149	6487.878	6469.416
6659.257	6713.616	6589.003	6566.896
6778.330	6844.341	6688.183	6661.396
6890.663	6973.973	6774.175	6743.614
6976.295	7081.452	6869.750	6813.378
8477.934	8529.504	8417.970	8408.100
8520.601	8571.738	8458.633	8439.140
8632.906	8687.243	8562.698	8535.644
8780.152	8855.503	8680.059	8650.810
8907.691	9007.997	8798.620	8750.244
10022.645	10081.841	9958.076	9948.572
10061.635	10104.834	10003.417	9980.371
10250.236	10316.373	10165.029	10136.843
10418.747	10481.696	10312.536	10266.390

Table S14. Main values of the *g* tensors of the low-lying Kramers doublets on Dy sites in Dy_4K_2 (3)

KD		Dy_4K_2			
		Dy1	**Dy2**	**Dy3**	**Dy4**
1	g_X	0.00035	0.00017	0.00020	0.00015
	g_Y	0.00065	0.00031	0.00044	0.00066
	g_Z	19.87240	19.88616	19.89088	19.89209
2	g_X	0.06954	0.03468	0.15575	0.18025
	g_Y	0.07114	0.03592	0.21510	0.22048
	g_Z	16.94751	16.99369	16.85995	16.81177
3	g_X	0.57325	0.44181	2.62866	1.77313
	g_Y	1.78029	0.92814	4.23986	2.85274
	g_Z	12.42735	13.35505	14.74993	14.32508
4	g_X	11.41083	2.09435	7.96154	2.62044
	g_Y	7.42237	6.33410	6.27037	5.97701
	g_Z	1.83320	13.02459	0.24656	9.87468
5	g_X	1.00691	0.53693	0.94255	1.61866
	g_Y	6.32846	3.46375	3.67886	4.03429
	g_Z	11.78614	14.80533	15.34001	13.29675
6	g_X	8.89072	6.69923	1.40466	10.60005
	g_Y	8.31116	5.82859	3.93152	6.83658
	g_Z	2.47042	1.93799	13.27594	1.95980
7	g_X	1.20534	10.78487	0.39506	0.55521
	g_Y	2.05934	7.13055	1.02456	3.38412
	g_Z	15.44389	2.17240	15.19077	13.17362
8	g_X	0.13318	0.45362	0.22503	0.43914
	g_Y	0.63348	0.87302	0.73547	4.13281
	g_Z	18.51937	18.73212	18.06292	15.23631

Table S15. Angle between the main magnetic axis of the ground Kramers doublets (KD 1) and the shortest chemical bond (Dy-O) of the corresponding Dy sites in Dy_4K_2 (3)

Dy_4K_2			
Dy1	**Dy2**	**Dy3**	**Dy4**
0.7045	0.6363	2.5132	2.6066

Comparison of the results in Tables S13-S15 and S9-S12 show that the electric field of surrounding molecules has minor effect on the electronic structure and magnetic anisotropy of individual Dy sites in the Dy_4K_2 (**3**) complex. Given that **1**-**5** and **7** are isostructural compounds, this conclusion is general for the whole series. The same is expected to be true for crystals of **6** and **8** which involve electroneutral species as well.

4.4 Ab initio calculations of Dy@7 and Dy@8 complexes

In these calculations (Tables S15-S17) the entire molecules $[DyY_3K_2O(O^tBu)_{12}]$ and $[DyY_4O(O^iPr)_{13}]$ have been considered in the experimental structures of $[Y_4K_2O(O^tBu)_{12}]$ **7** and $[Y_5O(O^iPr)_{13}]$ **8**, respectively, by replacing one of Y atoms with Dy without subsequent optimization of geometry. The numeration of Dy sites in the Tables S15-S17 is arbitrary and does not follow the numeration in Figure 1 and S9, as well as in Tables S9-S14

Table S16. Energies (cm^{-1}) of the low lying Kramers doublets in Dy@7 and Dy@8

DyY_3K_2				DyY_4				
Dy1	**Dy2**	**Dy3**	**Dy4**	**Dy1**	**Dy2**	**Dy3**	**Dy4**	**Dy5**
0.000	0.000	0.000	0.000	0.000	0.000	0.000	0.000	0.000
390.235	405.583	372.754	344.273	394.312	384.305	418.939	396.604	334.530
683.301	708.703	584.870	502.131	583.644	577.483	719.799	616.029	605.659
770.073	785.616	647.700	578.770	639.783	663.523	777.547	678.633	659.247
836.994	850.088	742.863	658.695	721.727	740.160	844.361	752.145	776.328
907.693	929.075	793.135	715.870	791.758	796.202	914.893	822.523	859.316
960.440	985.294	871.192	781.078	862.780	895.741	983.348	890.986	929.940
1065.858	1094.266	934.269	810.354	1042.173	1092.155	1124.498	1051.877	970.172
3755.678	3765.948	3745.886	3728.770	3760.714	3752.140	3773.929	3760.149	3710.410
4033.245	4052.233	3978.678	3934.305	3975.150	3985.084	4051.528	3988.750	4013.234
4197.810	4220.127	4123.486	4062.752	4118.920	4124.307	4221.213	4139.107	4143.503
4298.395	4314.246	4194.834	4124.631	4198.785	4207.040	4317.830	4229.852	4214.615
4370.111	4385.988	4256.135	4171.806	4240.827	4252.220	4372.433	4280.033	4283.781
4416.343	4422.122	4323.568	4232.606	4306.279	4338.361	4419.103	4335.631	4361.577
4495.362	4527.285	4364.055	4249.177	4442.376	4488.289	4547.993	4459.833	4399.039
6459.690	6478.832	6423.547	6391.095	6430.462	6434.069	6486.244	6437.525	6407.154
6562.809	6579.749	6501.934	6452.241	6494.391	6499.346	6573.462	6512.836	6531.642
6675.725	6686.773	6605.889	6546.391	6603.499	6611.743	6686.323	6622.514	6608.303
6799.971	6811.212	6710.882	6635.591	6715.107	6721.276	6813.054	6739.912	6706.617
6919.615	6934.208	6802.705	6712.703	6810.887	6828.071	6931.122	6842.063	6836.764
7014.222	7042.641	6892.702	6787.982	6917.926	6968.176	7051.088	6945.249	6942.787
8491.075	8509.130	8433.557	8391.542	8425.019	8440.308	8513.345	8441.551	8429.312
8533.218	8548.169	8471.606	8418.788	8468.541	8464.374	8537.346	8486.555	8492.948
8648.528	8655.665	8576.801	8511.823	8581.373	8591.142	8660.429	8599.395	8560.842
8804.538	8817.619	8703.817	8621.175	8715.084	8723.203	8817.241	8742.293	8709.041
8942.061	8967.789	8821.353	8722.497	8833.752	8881.868	8971.864	8862.508	8874.740
10038.280	10053.728	9972.281	9929.494	9962.404	9977.561	10055.813	9980.931	9970.792
10070.061	10081.357	10013.511	9957.679	10009.137	10003.568	10071.320	10026.661	10017.762
10269.748	10278.324	10183.906	10107.673	10193.431	10199.260	10281.154	10217.305	10156.933
10435.889	10449.030	10332.854	10236.827	10337.697	10367.951	10448.900	10365.405	10360.472

Table S17. Main values of the *g* tensors of the low-lying Kramers doublets in Dy@7 and Dy@8

KD		Dy_4K_2				Dy_5				
		Dy1	Dy2	Dy3	Dy4	Dy1	Dy2	Dy3	Dy4	Dy5
1	g_X	0.00020	0.00022	0.00012	0.00025	0.00020	0.00056	0.00032	0.00050	0.00012
	g_Y	0.00040	0.00044	0.00041	0.00073	0.00046	0.00081	0.00041	0.00060	0.00016
	g_Z	19.87823	19.87028	19.89600	19.87936	19.83604	19.87746	19.86657	19.86825	19.88257
2	g_X	0.04911	0.05269	0.13135	0.23444	0.03982	0.07604	0.02746	0.02256	0.06703
	g_Y	0.04993	0.05460	0.16823	0.32142	0.04378	0.09226	0.03086	0.03043	0.07784
	g_Z	16.97052	16.96160	16.88933	16.68985	16.72128	16.80269	16.97387	16.86979	17.01986
3	g_X	0.54097	0.94549	2.54477	1.59350	2.26111	1.26994	1.92975	1.48575	2.40610
	g_Y	1.29613	1.64473	4.69031	1.73606	5.88764	1.66725	2.55241	2.68248	6.84382
	g_Z	12.93600	12.66108	13.81831	16.11066	12.76310	16.66689	11.99496	14.59222	11.29910
4	g_X	2.01130	11.05313	8.00783	3.57903	0.93554	1.87066	1.09161	7.09843	7.33199
	g_Y	6.94571	8.39819	6.11737	6.58792	4.03818	4.37226	6.33386	6.30042	6.37660
	g_Z	12.04401	1.79324	0.54620	9.61405	8.05925	9.02879	11.84287	3.01292	2.96093
5	g_X	0.78364	1.51454	0.40502	1.87466	3.73046	1.23094	2.05249	1.75650	0.77251
	g_Y	5.37100	3.43376	3.93696	3.76500	4.05175	5.13421	2.75592	4.77412	3.88476
	g_Z	12.94232	14.21080	14.91404	13.36555	6.69974	11.25082	13.00124	8.87921	13.77051
6	g_X	7.81996	8.00561	1.74544	10.17299	8.28327	9.70388	9.78791	7.79215	4.01050
	g_Y	6.85462	6.09567	5.03111	7.18943	7.78398	6.32463	7.45764	7.61970	5.67952
	g_Z	1.18404	1.43405	12.64059	1.99033	2.83761	1.96715	2.75855	2.42346	9.70598
7	g_X	1.96655	10.78397	0.27588	0.86899	1.31043	0.84675	0.46374	1.40957	8.95290
	g_Y	4.27337	6.92598	0.97566	3.80099	2.01190	1.75910	1.72631	2.97516	7.39446
	g_Z	13.83775	1.97858	14.29053	13.05977	14.43825	15.53659	14.32960	13.88541	0.54680
8	g_X	0.22821	0.30084	0.33178	0.70056	0.02617	0.00429	0.17322	0.04884	11.42906
	g_Y	0.60738	0.79036	1.44061	4.87645	0.03237	0.07180	0.39931	0.14914	7.48137
	g_Z	18.76926	18.73594	17.18994	14.72203	19.26315	19.35248	19.10877	19.20879	1.36832

Table S18. Angle between the main magnetic axis of the ground Kramers doublets (KD 1) and the shortest chemical bond (Dy-O) of the corresponding Dy site in Dy@7 and Dy@8

Dy_4K_2				Dy_5				
Dy1	Dy2	Dy3	Dy4	Dy1	Dy2	Dy3	Dy4	Dy5
0.4840	0.3336	1.9677	1.6604	2.8280	1.1986	2.0548	1.6541	2.7227

To prove that the lack of geometry reoptimization in $[DyY_3K_2O(O^tBu)_{12}]$ and $[DyY_4O(O^iPr)_{13}]$ has no major influence on the calculated electronic structure and magnetic anisotropy on Dy sites, we performed similar calculations using the experimental geometry of complexes **3** and **6**, respectively, in which three and four Dy atoms have been replaced by Y. These data are available on request from the authors (L.U. and L.F.C.).

4.5 Magnetic interactions in {Dy_4K_2} (3) and {Dy_5} (6)complexes

Hamiltonian of the magnetic interactions for:

{Dy_4K_2} (numbering of the atoms as in Figure S12):

$$\boldsymbol{H_{exch} = -J_1\left(\widehat{s_{1,z}}\widehat{s_{2,z}} + \widehat{s_{1,z}}\widehat{s_{3,z}} + \widehat{s_{1,z}}\widehat{s_{4,z}} + \widehat{s_{2,z}}\widehat{s_{3,z}} + \widehat{s_{2,z}}\widehat{s_{4,z}}\right) + J_2\widehat{s_{3,z}}\widehat{s_{4,z}}}$$

{Dy_5}: (numbering of the atoms as in Figure S13):

$$\boldsymbol{H_{exch} = -J_1\left(\widehat{s_{1,z}}\widehat{s_{2,z}} + \widehat{s_{1,z}}\widehat{s_{3,z}} + \widehat{s_{1,z}}\widehat{s_{4,z}} + \widehat{s_{2,z}}\widehat{s_{3,z}} + \widehat{s_{2,z}}\widehat{s_{5,z}} + \widehat{s_{3,z}}\widehat{s_{4,z}} + \widehat{s_{3,z}}\widehat{s_{5,z}} + \widehat{s_{4,z}}\widehat{s_{5,z}}\right) -}$$

$$\boldsymbol{-J_2\left(\widehat{s_{1,z}}\widehat{s_{5,z}} + \widehat{s_{2,z}}\widehat{s_{4,z}}\right)}$$

where $\widehat{s_{i,z}}$ is the projection of the pseudospin s=1/2 on the main magnetic axis z of the centre i; J_1 and J_2 are the parameters of the total magnetic interaction between the centres (exchange and dipolar):

$$\boldsymbol{J_{total} = J_{exch} + J_{dip}}$$

Table S19 Magnetic dipolar and exchange couplings between Dy centres *Ising parameters (cm^{-1})* and the intramolecular transversal fields (Oe)

a { Dy_4K_2}

interaction	J_{dip}*	J_{exch}	$J_{total} = J_{dip}$* + J_{exch}	H_{ij}	H_{ji}
Dy1-Dy2	5.92975	-0.91479	5.01496	896.7	1369.0
Dy1-Dy3	-6.00701	1.49487	-4.51214	1478.4	922.5
Dy1-Dy4	6.34707	0.26872	6.61579	1528.9	745.2
Dy2-Dy3	6.48991	1.12451	7.61442	1248.2	1059.6
Dy2-Dy4	-6.01589	1.37456	-4.64133	1440.4	813.9
Dy3-Dy4	8.33448	-5.09818	3.23630	217.3	244.8

b { Dy_5}

interaction	J_{dip}*	J_{exch}	$J_{total} = J_{dip}$* + J_{exch}	H_{ij}	H_{ji}
Dy1-Dy2	-6.61069	-1.53727	-8.14796	737.9	2219.0
Dy1-Dy3	6.36798	-1.45983	4.90815	795.9	1807.2
Dy1-Dy4	6.45027	0.25415	6.70442	836.3	1541.7
Dy1-Dy5	3.49170	-4.88145	-1.38975	76.2	150.6
Dy2-Dy3	5.55638	-0.07987	5.47651	1959.1	612.4
Dy2-Dy4	2.67553	-4.89131	-2.21578	158.3	302.5
Dy2-Dy5	5.86642	-1.00116	4.86526	907.2	1595.5
Dy3-Dy4	-6.24080	-0.91447	-7.15528	1563.7	636.6
Dy3-Dy5	-6.40605	0.41076	-5.99529	1896.4	756.9
Dy4-Dy5	-6.62443	0.63967	-5.98476	1581.2	893.6

* -- contribution coming only from the Ising terms ~ $\hat{S}_{1,z}\hat{S}_{2,z}$ to the dipolar coupling. In the calculation of the exchange spectrum (Tables S19 and S20 respectively) the dipolar interaction included all terms.

** --H_{ij} is the transversal magnetic field created by Dy_i in the position Dy_j.

Table S20. Lowest exchange spectrum of the Dy_4K_2 (in cm^{-1}).

$J=J_{exch}+J_{dip}$			$J=J_{dip}$		
energy	Δ_{tun}	g_Z	energy	Δ_{tun}	g_Z
0.000000000	3.538590E-10	27.525523818	0.000000000	1.173870E-10	27.440034205
0.000000000			0.000000000		
2.971313583	4.285901E-10	51.422282236	1.472781465	8.557000E-11	51.316201645
2.971313583			1.472781465		
3.067342404	2.215099E-10	28.404848433	1.879456976	2.527001E-11	44.266930148
3.067342405			1.879456976		
3.610903030	2.486300E-10	25.536484820	3.212187422	8.656009E-11	28.323178931
3.610903030			3.212187423		
5.414813146	3.685052E-11	44.373901620	3.287929935	2.561995E-11	25.454701455
5.414813146			3.287929935		
6.501978734	1.442197E-10	50.102620087	4.607430095	1.181899E-10	49.993790060
6.501978734			4.607430095		
6.931473251	5.364500E-10	48.925513255	4.674332266	1.788898E-10	48.815889373
6.931473252			4.674332266		
11.725591810	3.237997E-10	31.495525351	12.429641312	1.800000E-10	31.410896631
11.725591810			12.429641312		
344.968253469	7.179892E-10	27.825050144	344.784129873	1.670060E-10	27.797617835
344.968253470			344.784129873		

Table S21. Lowest exchange spectrum (in cm^{-1}) of the Dy_5 (6) and the g_Z components of the g tensor of the corresponding Kramers doublet (g_X, g_Y<10^{-6}).

$J=J_{exch}+J_{dip}$		$J=J_{dip}$	
energy	g_Z	energy	g_Z
0.000000000	26.114782461	0.000000000	14.393483420
0.000000000		0.000000000	
0.807008193	14.393483516	0.488426364	14.393483420
0.807008193		0.488426364	
3.042402661	49.363503859	1.784972086	26.114782276
3.042402661		1.784972086	
4.606552166	44.524087007	2.079182042	49.363504112
4.606552166		2.079182042	
5.492440497	40.624136684	2.089065767	44.524086431
5.492440497		2.089065767	
5.566099360	40.570052480	2.122600791	40.624137324
5.566099360		2.122600791	
7.353770718	18.083946187	3.157353283	40.570052220
7.353770718		3.157353283	
7.653256269	60.472901914	3.480530364	60.472903760
7.653256269		3.480530364	
7.948770354	60.551487503	3.597534485	60.551488363
7.948770354		3.597534485	
8.377855755	59.601220610	3.958780924	59.601223276
8.377855755		3.958780924	
9.718032641	56.510898211	6.877313451	56.510899439
9.718032641		6.877313451	
9.866975268	45.891302140	7.702599000	18.083946936
9.866975268		7.702599000	
10.243487591	46.355350332	7.968623351	45.891302290
10.243487591		7.968623351	
10.919631192	46.216558089	8.167407655	41.084196427
10.919631192		8.167407655	
11.272350859	41.084196375	8.808412447	46.355352384
11.272350859		8.808412447	
19.151245392	22.554054168	19.162924313	46.216558943
19.151245392		19.162924313	

4.4 Magnetic properties of the $\{Dy_4K_2\}$ (3) and $\{Dy_5\}$ (6) complexes

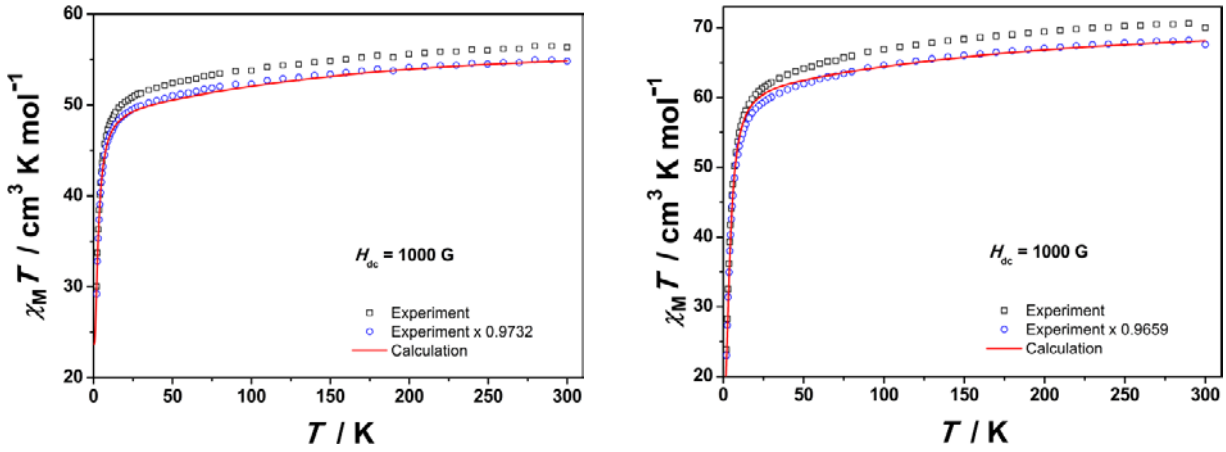

Figure S14 Measured (empty figures) and calculated (red line) molar magnetic susceptibility of the $\{Dy_4K_2\}$ (left) and $\{Dy_5\}$ (right) complexes.

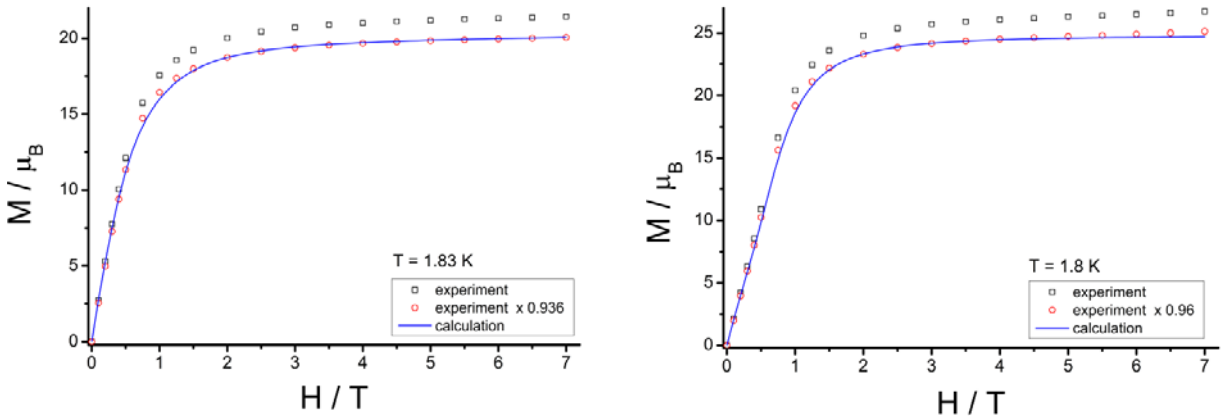

Figure S15 Measured (empty figures) and calculated (blue line) molar magnetization at 1.8 K of the $\{Dy_4K_2\}$ (left) and $\{Dy_5\}$ (left) molecules.

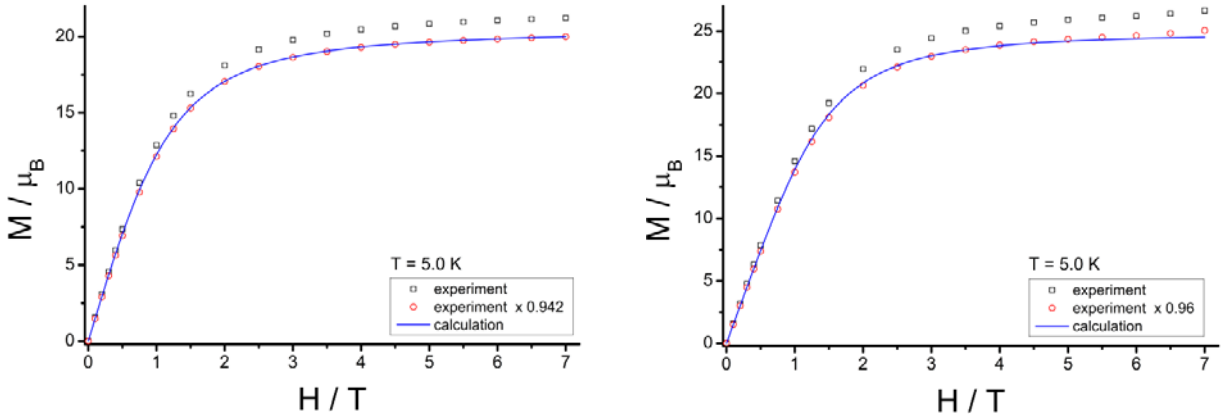

Figure S16 Measured (empty figures) and calculated (blue line) molar magnetization at 5.0 K of the $\{Dy_4K_2\}$ (left) and $\{Dy_5\}$ (left) molecules.

Table S22 Averaged matrix elements of squares of magnetic moment $\left(\overline{\langle i|\mu|j\rangle}\right)^2$ [a,b] (in μ_B^2)

i,j	Dy1	Dy2	Dy3	Dy4	Dy5
			{Dy_4K_2}		
(1-,3+)	4.291×10^{-4}	8.520×10^{-5}	1.124×10^{-2}	3.549×10^{-3}	
(1-,2+)	3.221×10^{-7}	1.023×10^{-7}	6.312×10^{-6}	2.142×10^{-6}	
(1-,1+)	3.229×10^{-8}	1.195×10^{-8}	1.510×10^{-8}	3.086×10^{-8}	
(1-, 2-)	4.613	4.644	4.608	4.595	
(1-,3-)	3.428×10^{-3}	1.380×10^{-3}	4.722×10^{-3}	1.935×10^{-2}	-
(2-,3+)	7.604×10^{-3}	1.681×10^{-3}	1.193	2.881×10^{-1}	
(2-,2+)	6.555×10^{-4}	1.920×10^{-4}	4.625×10^{-3}	7.227×10^{-3}	
(2-,3-)	7.653	24.07	2.826	4.331	
(3-,3+)	4.668×10^{-1}	7.675×10^{-2}	2.055	6.707×10^{-1}	
			{Dy_5}		
(1-,3+)	2.442×10^{-4}	6.141×10^{-8}	5.517×10^{-6}	1.698×10^{-4}	7.993×10^{-3}
(1-,2+)	1.300×10^{-6}	6.011×10^{-10}	7.929×10^{-9}	1.054×10^{-6}	3.714×10^{-5}
(1-,1+)	5.851×10^{-8}	4.500×10^{-11}	6.196×10^{-10}	5.270×10^{-8}	5.628×10^{-7}
(1-, 2-)	4.662	4.657	4.650	4.596	4.612
(1-,3-)	2.872×10^{-2}	3.424×10^{-3}	4.576×10^{-3}	2.212×10^{-2}	5.213×10^{-2}
(2-,3+)	8.238×10^{-3}	2.047×10^{-6}	1.245×10^{-4}	2.860×10^{-3}	5.390×10^{-1}
(2-,2+)	9.761×10^{-4}	3.418×10^{-7}	2.108×10^{-5}	2.765×10^{-4}	2.388×10^{-2}
(2-,3-)	7.268	8.514	8.460	7.917	3.363
(3-,3+)	9.178×10^{-2}	6.618×10^{-4}	1.794×10^{-3}	2.825×10^{-2}	6.099×10^{-1}

a) Calculated as arithmetic mean of squares of three Cartesian Components: $\left(|\mu_X|^2 + |\mu_Y|^2 + |\mu_Z|^2\right)/3$

b) $\left(\overline{\langle i+|\mu|j-\rangle}\right)^2 = \left(\overline{\langle i-|\mu|j+\rangle}\right)^2$

$\left(\overline{\langle i+|\mu|j+\rangle}\right)^2 = \left(\overline{\langle i-|\mu|j-\rangle}\right)^2$

4.5 Ab initio studies of the {Ho_4K_2} and {Er_4K_2} complexes

Table S23 Energies (cm^{-1}) of the low lying energy levels in compounds {Ho_4K_2} **4** and {Er_4K_2} **5**.

Ho_4K_2				Er_4K_2			
Ho1	**Ho2**	**Ho3**	**Ho4**	**Er1**	**Er2**	**Er3**	**Er4**
0.000	0.000	0.000	0.000	0.000	0.000	0.000	0.000
0.010	0.000	0.002	0.005	30.159	37.985	23.199	23.126
272.731	362.710	346.961	283.174	59.555	75.670	51.557	59.167
277.553	363.533	347.858	286.554	97.524	116.756	103.213	96.222
288.184	376.711	359.913	295.561	162.736	167.182	161.279	148.976
296.147	378.362	362.065	299.222	189.686	186.809	180.520	151.986
312.186	394.434	385.102	334.490	233.522	198.527	196.510	200.266
314.338	396.590	387.560	336.259	490.167	718.228	574.236	505.957
352.834	430.072	415.042	351.410	6592.175	6589.143	6580.712	6595.353
360.162	438.598	426.910	360.108	6614.047	6629.857	6609.594	6608.859
383.460	441.965	439.381	386.315	6649.388	6660.479	6647.493	6644.333
398.769	465.012	475.699	410.623	6700.833	6696.638	6692.301	6681.870
405.416	469.144	483.335	417.373	6730.971	6713.205	6718.757	6710.554
437.707	519.130	512.737	452.093	6749.908	6768.936	6749.615	6729.313
446.268	522.758	517.900	462.148	6962.660	7145.722	7031.903	6974.254
458.964	545.958	538.450	465.785	10644.630	10645.176	10634.464	10646.763
463.204	546.915	539.140	471.401	10665.752	10677.821	10661.974	10660.047
5199.109	5226.763	5220.918	5200.808	10704.635	10703.799	10697.135	10691.877
5199.112	5226.764	5220.919	5200.812	10732.688	10724.202	10721.040	10713.310
5355.017	5406.578	5398.833	5359.913	10746.618	10774.146	10755.236	10734.618
5355.559	5406.948	5399.267	5360.553	10899.216	11038.512	10952.526	10906.726
5414.716	5497.810	5483.324	5422.999	13405.142	13411.937	13415.902	13404.236
5420.956	5504.391	5489.386	5429.277	13456.469	13458.485	13446.411	13458.462
5432.774	5511.693	5501.044	5445.894	13503.363	13497.787	13488.880	13482.034
5441.374	5525.552	5513.393	5460.112	13559.673	13568.608	13553.259	13545.425
5456.834	5530.668	5525.182	5470.527	13672.257	13789.266	13714.114	13677.276
5465.892	5540.257	5535.527	5474.286	18909.673	18800.800	18849.997	18904.100
5478.297	5549.716	5547.656	5485.777	18965.360	18899.114	18931.446	18944.380
5504.996	5583.262	5576.804	5520.158	19043.599	19051.973	19047.771	19036.798
5507.462	5583.973	5578.804	5525.084	19156.991	19237.403	19191.182	19162.785
5524.431	5608.162	5603.444	5525.633				
5525.541	5608.381	5603.768	5528.827				
8920.579	8959.424	8950.309	8922.697				
8920.607	8959.434	8950.322	8922.720				
9029.707	9069.978	9066.079	9035.596				
9030.001	9070.256	9066.316	9036.060				
9104.378	9180.706	9170.207	9112.144				
9117.380	9194.812	9183.888	9124.960				
9125.144	9213.706	9200.588	9141.262				
9138.477	9224.323	9211.117	9153.488				
9148.824	9227.506	9217.752	9161.904				
9167.913	9240.228	9233.609	9180.613				
9177.080	9253.689	9245.296	9190.789				
9194.471	9276.145	9272.937	9198.397				
9195.927	9278.034	9274.057	9201.429				
11690.189	11731.428	11721.765	11693.004				
11690.570	11731.738	11722.038	11693.207				
11799.860	11843.899	11839.305	11806.472				
11802.948	11845.953	11841.565	11809.628				
11871.572	11958.980	11945.731	11881.345				

Table S24 Main values of the *g* tensors of the low-lying energy levels on Ln sites in compounds {Ho_4K_2} **4** and {Er_4K_2} **5**.

		Ho_4K_2						Er_4K_2			
ID		**Ho1**	**Ho2**	**Ho3**	**Ho4**	**KD**		**Er1**	**Er2**	**Er3**	**Er4**
1	g_X	19.85417	19.87522	19.85427	19.83310	**1**	g_X	1.26792	0.51498	0.50028	1.71171
	g_Y						g_Y	3.77364	1.12087	1.14278	5.12203
	g_Z						g_Z	13.77721	16.77095	16.69809	12.29031
2	g_X	14.87757	16.48829	16.73462	15.65366	**2**	g_X	1.21782	0.73606	1.65190	1.63488
	g_Y						g_Y	4.94463	1.71914	1.92622	2.92830
	g_Z						g_Z	10.74206	14.00208	14.28618	10.59715
3	g_X	-	-	-	-	**3**	g_X	1.21236	0.54375	1.39661	0.77452
	g_Y						g_Y	4.55403	3.51499	1.73790	4.00965
	g_Z						g_Z	9.37526	11.19640	11.68047	9.63471
4	g_X	-	-	-	-	**4**	g_X	3.05986	3.99349	7.41897	3.77706
	g_Y						g_Y	3.16448	4.81602	6.58230	4.04628
	g_Z						g_Z	10.17559	9.41575	4.47194	9.44172
5	g_X	-	-	-	-	**5**	g_X	0.11317	1.98600	0.21569	0.09408
	g_Y						g_Y	0.41141	3.26976	2.06669	4.74940
	g_Z						g_Z	14.42163	8.89672	10.29836	10.71696
6	g_X	-	-	-	-	**6**	g_X	0.16114	0.17977	0.76957	10.13044
	g_Y						g_Y	0.46650	2.59604	1.30193	5.42046
	g_Z						g_Z	16.57236	10.49622	14.22113	0.55170
7	g_X	-	-	-	-	**7**	g_X	0.21057	0.11102	0.93435	0.04689
	g_Y						g_Y	0.48325	2.27513	1.58293	0.15389
	g_Z						g_Z	16.95857	11.47949	14.99448	17.29847
8	g_X	-	-	-	-	**8**	g_X	0.00658	0.00007	0.00034	0.00234
	g_Y						g_Y	0.00780	0.00017	0.00041	0.00300
	g_Z						g_Z	17.89511	17.93272	17.94437	17.93986

Table S25 Angle between the main magnetic axis of the ground and first excited levels in compounds {Ho_4K_2} **4** and {Er_4K_2} **5**.

Ho_4K_2				Er_4K_2			
Ho1	**Ho2**	**Ho3**	**Ho4**	**Er1**	**Er2**	**Er3**	**Er4**
56.4281	5.6603	16.9774	26.3688	64.5552	83.5395	72.9941	36.1789

Table S26 Angle between the main magnetic axis of the ground level and the shortest chemical bond (Ln-O) of the corresponding Ln site in compounds {Ho_4K_2} **4** and {Er_4K_2} **5**.

{Ho_4K_2}				{Er_4K_2}			
Ho1	**Ho2**	**Ho3**	**Ho4**	**Er1**	**Er2**	**Er3**	**Er4**
4.9970	1.6215	3.1020	6.4301	61.0820	86.5381	83.1445	68.7804

4.6 Magnetic interactions in {Ho_4K_2} and {Er_4K_2} complexes

Hamiltonian of the magnetic interactions for:
Ho_4K_2 (numbering of the atoms as in Figure 3):

$$\boldsymbol{H_{exch} = -J_1\left(\widehat{s_{1,z}}\widehat{s_{2,z}} + \widehat{s_{1,z}}\widehat{s_{3,z}} + \widehat{s_{1,z}}\widehat{s_{4,z}} + \widehat{s_{2,z}}\widehat{s_{3,z}} + \widehat{s_{2,z}}\widehat{s_{4,z}}\right) + J_2\widehat{s_{3,z}}\widehat{s_{4,z}}}$$

where $\widehat{s_{i,z}}$ is the projection of the pseudospin s=1/2 on the main magnetic axis z of the centre i; J_1 and J_2 are the parameters of the total magnetic interaction between the centres (exchange and dipolar):

$$\boldsymbol{J_{total} = J_{exch} + J_{dip}}$$

Table S27 Magnetic dipolar and exchange couplings in {Ho_4K_2} *Ising parameters (cm^{-1}):*

interaction	J_{dip}^*	J_{exch}	$J_{total} = J_{dip}^* + J_{exch}$
Ho1-Ho2	6.51171	-0.99002	5.52169
Ho1-Ho3	-6.27089	-0.86086	-7.13175
Ho1-Ho4	3.17299	-5.74309	-2.57011
Ho2-Ho3	6.21417	0.22838	6.44255
Ho2-Ho4	-6.30266	-0.56329	-6.86595
Ho3-Ho4	6.44874	-0.43181	6.01693

* -- contribution coming only from the Ising terms ~$\hat{\tilde{s}}_{1,z}\hat{\tilde{s}}_{2,z}$ to the dipolar coupling. In the calculation of the exchange spectrum (Tables S26 and S27 respectively) the dipolar interaction included all terms.

For Er_4K_2 only dipolar coupling was considered. No fitting of the exchange part was done.

Table S28. Lowest exchange spectrum of the Ho_4K_2 (in cm^{-1}).

$J=J_{exch}+J_{dip}$			$J=J_{dip}$		
energy	Δ_{tun}	g_z	energy	Δ_{tun}	g_z
0.000000000 0.000001695	1.695677E-06	28.328146270	0.000000000 0.000001696	1.696043E-06	28.378570851
3.014003984 3.014004222	2.383051E-07	46.489846950	1.593052819 1.593053170	3.509516E-07	28.378570851
3.103536979 3.103537346	3.667094E-07	26.831144117	1.786327498 1.786327737	2.391263E-07	50.298970868
3.307693046 3.307694003	9.572328E-07	28.770363597	3.252856318 3.252857276	9.574234E-07	46.595312681
3.688260947 3.688261299	3.515961E-07	50.227671718	3.300162338 3.300162706	3.673531E-07	28.818708976
6.504365446 6.504366423	9.767752E-07	48.540559303	4.788845570 4.788846660	1.089564E-06	26.877797846
6.552400438 6.552401528	1.089788E-06	48.880164671	4.804465770 4.804466748	9.777273E-07	48.950447504
12.765522937 12.765523308	3.709090E-07	28.332403580	12.766854855 12.766855226	3.712489E-07	48.611621227
274.944166618 274.944167807	1.188766E-06	24.187098982	275.082058189 275.082059566	1.377187E-06	28.383740843

Table S29. Lowest exchange spectrum of the Er_4K_2 (in cm^{-1}).

$J=J_{dip}$		
energy	Δ_{tun}	g_Z
0.000000000 0.002302064	2.302064E-03	14.495683968
0.514446144 0.515845900	1.399756E-03	26.403576694
0.697307690 0.702583436	5.275746E-03	26.158335179
1.635097403 1.641036644	5.939240E-03	43.044313635
1.863029255 1.864438348	1.409093E-03	11.535728369
2.967433230 2.977633259	1.020003E-02	19.612549606
3.026975453 3.036873032	9.897579E-03	25.535570655
4.915958902 4.916752458	7.935556E-04	38.502972005
23.220784477 23.223316751	2.532275E-03	16.062974930

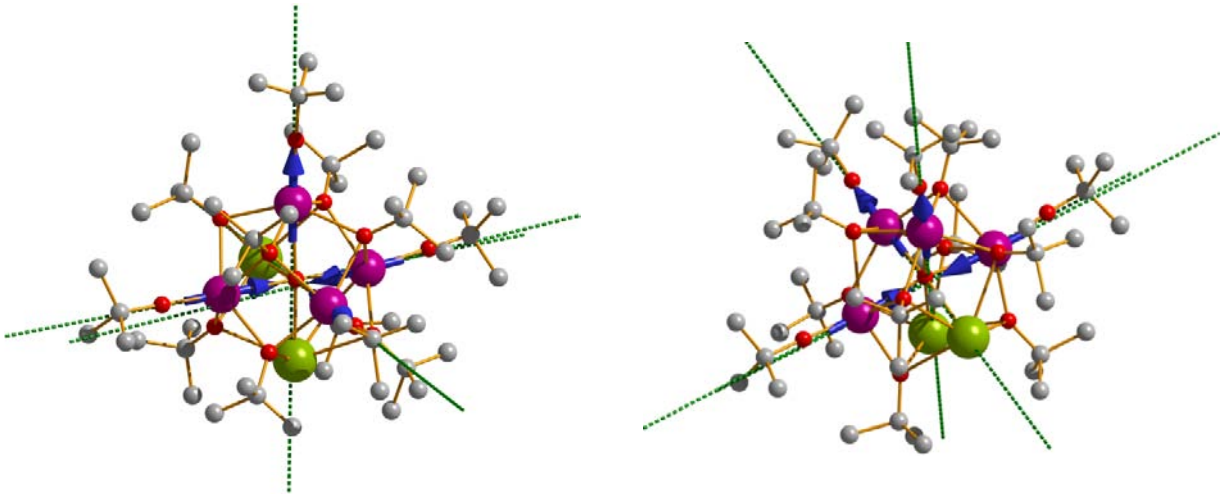

Figure S17 Orientations of local magnetic moments on Ho centres in the ground state of the $\{Ho_4K_2\}$ molecule.

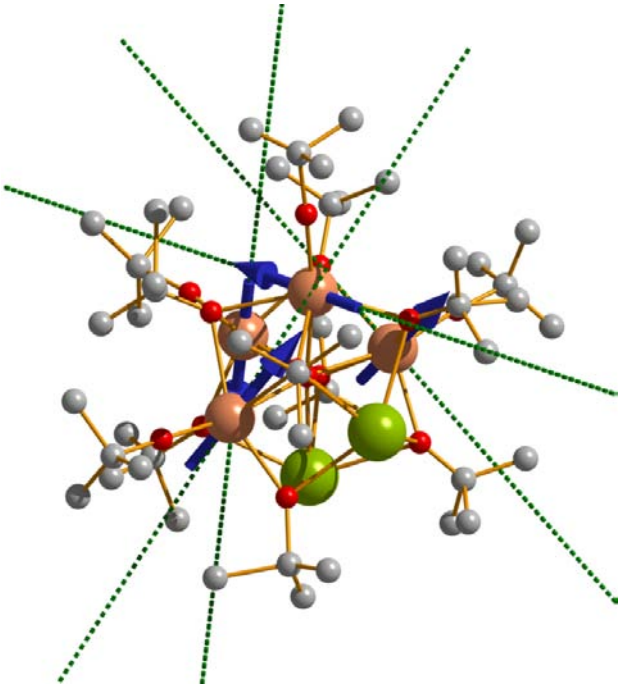

Figure S18 Orientations of local magnetic moments on Er centres in the ground state of the $\{Er_4K_2\}$ molecule.

4.7 Magnetic properties of the $\{Ho_4K_2\}$ and $\{Er_4K_2\}$ complexes

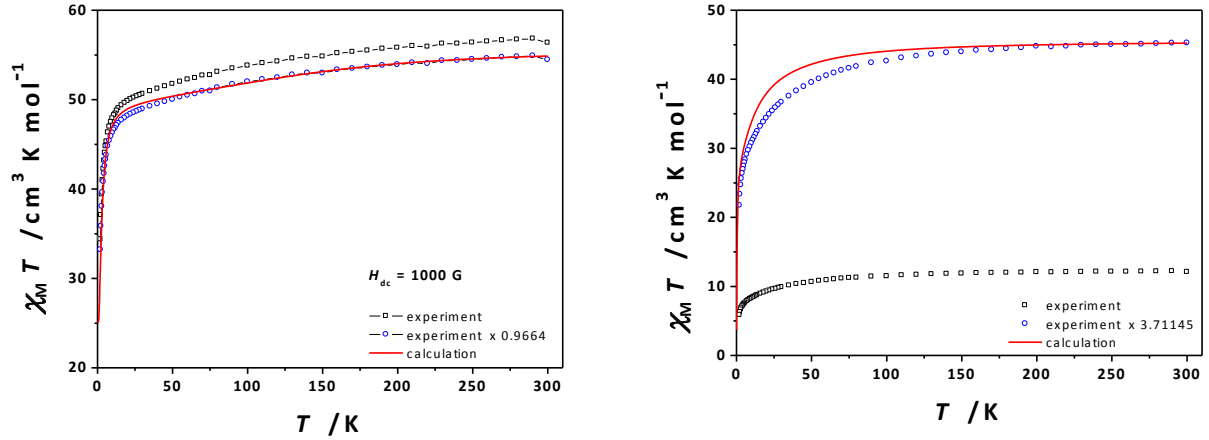

Figure S19 Measured (empty figures) and calculated (red line) molar magnetic susceptibility of the $\{Ho_4K_2\}$ (left) and $\{Er_4K_2\}$ (right) complexes.

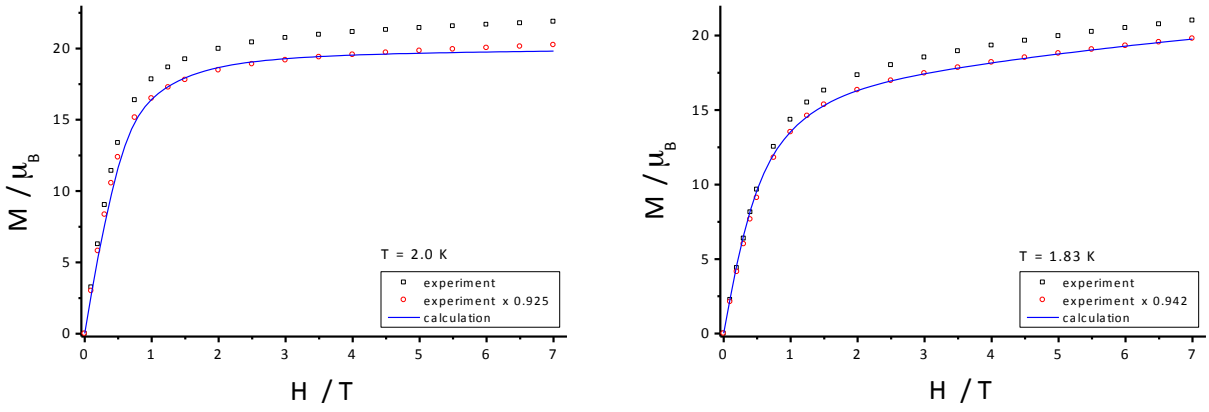

Figure S20 Measured (empty figures) and calculated (blue line) molar magnetization at indicated temperatures of the $\{Ho_4K_2\}$ (left) and $\{Er_4K_2\}$ (right) molecules.

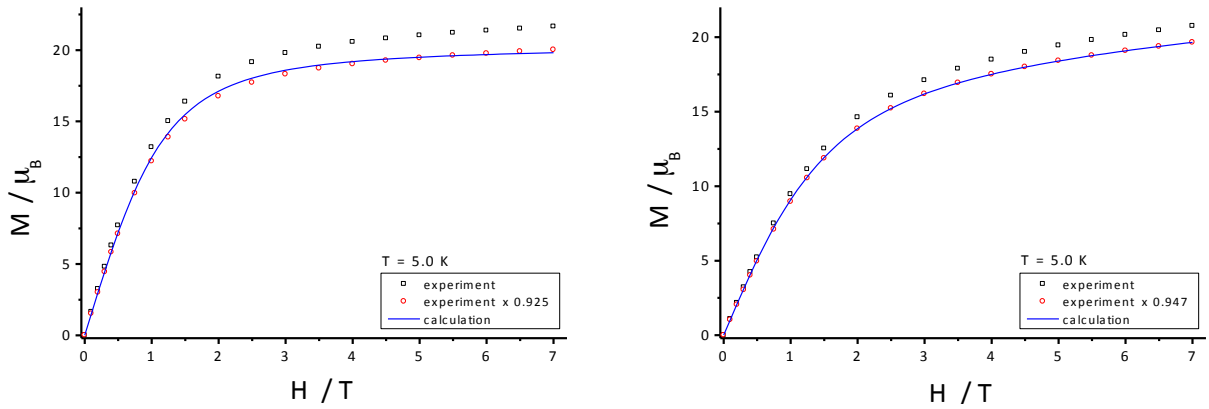

Figure S21 Measured (empty figures) and calculated (blue line) molar magnetization at 5.0 K of the $\{Ho_4K_2\}$ (left) and $\{Er_4K_2\}$ (right) molecules.

5.0 References

(PSH+1989) O. Poncelet, W. J. Sartain, L. G. Hubert-Pfalzgraf, K. Folting and K. G. Caulton, *Inorg. Chem.*, 1989, **28**, 263-267.

(PSLP1991) C. J. Page, S. K. Sur, M. C. Lonergan and G. K. Parashar, *Magn. Reson. Chem.*, 1991, **29**, 1191-1195.

(DLS-I19) H. Nowell, S. A. Barnett, K. E. Christensen, S. J. Teat and D. R. Allan, 2012, **19**, 435-441.

(XRAY-SHELX) G. M. Sheldrick , *Acta Cryst.*, 2008, **A64**, 112-122.

(XRAY-OLEX2) O. V. Dolomanov, L. J. Bourhis, R. J. Gildea, J. A. K. Howard and H. Puschmann , *J. Appl. Cryst.*, 2009, **42**, 339-341.

(XRAY-OLEX.SOLVE) L. J. Bourhis, O. V. Dolomanov, R. J. Gildea, J. A. K. Howard and H. Puschmann, in preparation.